Published in final edited form as:

Neuron. 2023 August 16; 111(16): 2488–2501.e8. doi:10.1016/j.neuron.2023.05.015.

Labeling PIEZO2 activity in the peripheral nervous system

Nicholas W. Villarino[1,2], **Yasmeen M. F. Hamed**[3,4], **Britya Ghosh**[3], **Adrienne E. Dubin**[1], **Amanda H. Lewis**[5], **Max A. Odem**[3], **Meaghan C. Loud**[1,2], **Yu Wang**[1], **M. Rocio Servin-Vences**[1], **Ardem Patapoutian**[1,2,*], **Kara L. Marshall**[1,2,3,6,*]

[1]Department of Neuroscience, Dorris Neuroscience Center, The Scripps Research Institute, La Jolla, CA 92037.

[2]Howard Hughes Medical Institute, The Scripps Research Institute, La Jolla, CA 92037.

[3]Department of Neuroscience, Baylor College of Medicine, Houston TX 77030.

[4]Graduate Program in Development, Disease Models, and Therapeutics, Baylor College of Medicine, Houston TX 77030.

[5]Department of Neurobiology, Duke University Medical Center, Durham NC, 27710.

[6]Jan and Dan Duncan Neurological Research Institute at Texas Children's Hospital, Houston, TX, 77030.

SUMMARY

Sensory neurons detect mechanical forces from both the environment and internal organs to regulate physiology. PIEZO2 is a mechanosensory ion channel critical for touch, proprioception and bladder stretch sensation, yet its broad expression in sensory neurons suggests it has undiscovered physiological roles. To fully understand mechanosensory physiology, we must know where and when PIEZO2-expressing neurons detect force. The fluorescent styryl dye FM 1–43 was previously shown to label sensory neurons. Surprisingly, we find that the vast majority of FM 1–43 somatosensory neuron labeling in mice *in vivo* is dependent on PIEZO2-activity within the peripheral nerve endings. We illustrate the potential of FM 1–43 by using it to identify novel *Piezo2*-expressing urethral neurons that are engaged by urination. These data reveal that FM 1–43 is a functional probe for mechanosensitivity via PIEZO2 activation *in vivo* and will facilitate the characterization of known and novel mechanosensory processes in multiple organ systems.

eTOC blurb

[*]co-corresponding authors: A.P.: ardem@scripps.edu, Lead contact: K.L.M: kara.marshall@bcm.edu.

Author Contributions

Conceptualization: N.W.V., A.P., K.L.M, Validation, N.W.V., M.A.O., K.L.M., Formal Analysis, N.W.V., Y.M.F.H, B.G., A.E.D., A.H.L., M.A.O., K.L.M., Investigation: N.W.V., Y.M.F.H, B.G., A.E.D., A.H.L., M.A.O., M.C.L., Y.W., M.R.S-V, K.L.M., Writing–Original Draft: N.W.V, A.E.D., A.P., K.L.M., Writing– Review and Editing: all authors, Visualization, N.W.V., Y.M.F.H, B.G., A.E.D., A.H.L., M.A.O., K.L.M., Supervision: A.P., K.L.M.

Declaration of Interests

The authors declare no competing interests.

Mechanosensory processes are critical for the function of many organ systems. Villarino et al. find that the fluorescent dye FM 1–43 specifically labels the activity of the mechanosensitive ion channel PIEZO2 in mouse sensory neurons *in vivo*. This tool enables characterization of mechanosensory processes that rely on this important mechanosensor.

INTRODUCTION

Knowing when and where the nervous system detects mechanical force remains a challenge. The mechanosensory ion channel PIEZO2 is expressed in the peripheral nervous system, where it detects mechanical forces to mediate the senses of touch, proprioception, lung stretch, baroreception, and bladder fullness [1–6]. There are no known endogenous or exogenous chemical agonists for PIEZO2, so identifying where PIEZO2 is expressed is an important clue that a specific cell or tissue may detect mechanical force. Unfortunately, antibodies against PIEZO2 or a PIEZO2-GFP knock-in mouse [4] have had limited efficacy for *in vivo* localization of PIEZO2. To aid in visualizing mechanosensory endings that might express PIEZO2, we turned to the fluorescent styryl dye FM 1–43 [7]. This dye partitions into lipid membranes and has been used to study vesicular recycling, but also is proposed to enter cells through a separate mechanism: sensory ion channel permeation [8]. This feature has enabled the study of mechanotransduction ion channel activity in cochlear hair cells, and others have noted cell labeling in cell culture that is dependent on expression of TRPA1, TRPV1, and P2X ion channels [8,9]. Following these discoveries, FM 1–43 was used as a nonspecific sensory cell labeling tool in a wide variety of contexts [10–13]. This dye is reported to permeate mechanosensory channels in sensory neurons of the dorsal root ganglia (DRG) [14], indicating that it should label PIEZO2 positive endings.

RESULTS

We thus set out to determine how much of *in vivo* FM 1–43 labeling in sensory neurons depends on PIEZO2, the primary mechanotransduction channel expressed by DRG neurons. Constitutive knockout (KO) of *Piezo2* in all tissues is lethal, so we used a Cre recombinase driven by the segmentation gene *HoxB8* to delete functional *Piezo2* from caudal tissues only [4,15]. $HoxB8^{Cre}$ expression begins in the lower cervical regions and increases to full expression in thoracic levels [15]. Bright cell body labeling was seen in DRGs 24 hours after an intraperitoneal injection of FM 1–43 FX (1.12 mg/kg). Throughout this manuscript we use FM 1–43 as a shorthand for the analog known as FM 1–43FX or AM 1–43, which has superior fixation qualities (Figure S1A–B). To our surprise, the widespread labeling of DRG cell bodies was nearly absent from the caudal DRGs in $HoxB8^{Cre+};Piezo2^{f/f}$ mice 24 h after FM 1–43 injection (Figure 1A, Figure S1C,D). Quantification of DRG labeling revealed a gradient of decreasing fluorescence in $HoxB8^{Cre+};Piezo2^{f/f}$-KO ganglia that corresponds well to the increasing rostral-to-caudal gradient of $HoxB8^{Cre}$ expression (Figure 1B). Some FM 1–43 was visible in caudal *Piezo2*-KO DRGs which is possibly due to sparse *Piezo2* transcript observed in $HoxB8^{Cre+};Piezo2^{f/f}$-KO mice [16]. Additionally, FM 1–43 was frequently visible in the vasculature (Figure S1E–G), however, this vascular labeling diminishes by 24 h (Figure 1A) and may reflect the endocytic activity of the endothelium and/or labeling of the outer leaflet of the endothelial lumen. We also used

Phox2b^{Cre+};*Piezo2*$^{f/f}$ animals to remove functional *Piezo2* from the nodose ganglion, which supplies sensory innervation to the major organs of the body via the vagus nerve. Nodose neuronal cell body labeling was virtually absent in the KO animals, whereas the labeling in the adjacent jugular ganglion, which is not targeted by *Phox2b*^{Cre}, remained (Figure 1C–D). Together, these data reveal that the majority of FM 1–43 sensory neuron labeling is dependent on PIEZO2 expression.

Mechanotransduction sites are located in peripheral sensory neuron endings, which are distant from cell bodies in the DRG and nodose ganglion. Injection of FM 1–43 *in vivo* robustly labels peripheral sensory endings in addition to sensory neuron cell bodies. To investigate sensory endings supplied by the nodose ganglion, we surveyed the baroreceptor endings that wrap around the central arch of the aorta to detect blood pressure [6,17] (Figure 1E). Min et al. (2019) and others have shown that PIEZO2 positive afferents are only a subset of neurons that innervate the aortic arch [18]. Consistent with this, we see a subset of aortic arch neurons labeled by FM 1–43 (Figure S1H). These endings were not labeled in *Phox2b*$^{Cre+}$;*Piezo2*$^{f/f}$ animals injected with FM 1–43 (Figure 1F–G). Our previous work showed that baroreceptor endings are still present in *Piezo2*-KO animals and still functional because of redundancy provided by the related mechanotransduction ion channel PIEZO1 [6]. Given that we see complete loss of aortic arch labeling and nodose neuron labeling in *Piezo2* KO animals, this suggests that *in vivo* FM 1–43 labeling in sensory neurons depends on *Piezo2* expression, but not *Piezo1*, which is expressed in some nodose neurons [18].

Another example of robust FM 1–43 labeling occurs in cutaneous end organ structures of the hairy skin, which surround follicles to detect various stimulus modalities to ultimately convey the sense of touch [19,20]. Lanceolate, circumferential, and Merkel-cell neurite complexes frequently label 24 h post i.p. FM 1–43 injection (Figure 1H–I). Consistent with what we observed in DRGs, labeling of these terminal endings on hind-leg skin was absent in *HoxB8*$^{Cre+}$;*Piezo2*$^{f/f}$ mice (Figure 1J–L), though the underlying innervation remains intact, as marked by neurofilament heavy chain (NFH) immunostaining (Figure 1J).

If FM 1–43 permeates PIEZO2-positive neurons at the site of mechanotransduction, then it should enter first at the peripheral sensory endings, and only label cell bodies after sufficient time for trafficking back from the periphery. In the highly active baroreceptor endings, we did observe labeling at the periphery before the nodose cell bodies (1.5 h versus 6 h; Figure S1I–L). Robust DRG cell body labeling was only seen 12 h after injection, consistent with them being farther from their peripheral endings than nodose cell bodies (Figure S1 M–O). Remarkably, this labeling remained bright even after 7 weeks (Figure S1P). We also used a multiple timepoint, dual labeling strategy with FM 1–43 and FM 4–64, which has identical labeling patterns to FM 1–43 (Figure S2A–C), to parse regional differences in labeling timing (Figure S2D–F). This allows us to see regions within a nerve ending structure that label more robustly at early timepoints. Together, these data indicate that dye labeling is first occurring at sites of sensory transduction before being trafficked back to cell bodies where labeling persists.

Our results clearly demonstrate the PIEZO2-dependent labeling in DRGs, however, PIEZO2 is expressed in a large fraction of DRG neurons of numerous sensory subtypes.

We characterized subpopulations of sensory neurons labeled by FM 1–43 by assessing colocalization with immunostaining of DRG subtype markers 48 h post-injection, which is brighter than 24 h (Figure S1O). Using markers of myelinated Aβ and Aδ-low threshold mechanoreceptors (LTMRs) [20,21], we found 50.6% ± 9.7 of NFH-positive DRGs take up FM 1–43 (Figure 2A, G), and 68.3 % ± 5.2 of neurons expressing calbindin, a marker for Aβ RA-LTMRs [22], accumulate FM 1–43 (Figure 2B, H). Interestingly, up to 95% ± 3 of the tyrosine hydroxylase (TH) population, a marker for unmyelinated c-LTMRs, co-labels with FM 1–43 (Figure 2C, I)[23]. This indicates that FM 1–43 labels a large portion of innocuous mechanoreceptors, which are known to depend on PIEZO2 to convey the sense of touch [3,24]. PIEZO2 transcript has also been identified in some nociceptors, which could contribute to FM 1–43 accumulation [16,25]. To mark peptidergic and nonpeptidergic nociceptive populations, we stained for the nerve growth factor TRKA, calcitonin gene-related peptide (CGRP), and isolectin B4 [26,27]. Among FM 1–43 labeled neurons, low overlap is observed with peptidergic, TRKA (0.6% ± 0.6) and CGRP (3.3% ± 2.6) (Figure 2D–E, 2J–K), and non-peptidergic nociceptors, IB4 (2.2% ± 1.8) (Figure 2F, L). The predominant role for PIEZO2 in healthy tissues is to convey innocuous mechanosensation rather than pain [2,3,24]. Together, these results indicate that *Piezo2*-dependent FM 1–43 labeling overlaps with neuronal types that engage PIEZO2 activity, rather than simple expression patterns.

Terminal end organ structures in hairy skin are organized to relay distinct sensory information and consist of many neuronal subpopulations [19,20,28]. FM 1–43 frequently labels both longitudinal lanceolate and circumferential endings (Figure 1H) of hair follicles, and we sought to broadly examine subtype labeling patterns by immunostaining. Colocalization of FM 1–43 and markers was determined by assessing percent voxel overlap between dye and respective markers around guard hair follicles. As expected, we observed frequent overlap of myelinated endings labeling with NFH [29]; 45% of FM dye signal overlapped with NFH, and of total NFH signal, 51% overlapped with FM 1–43 (Figure 3A, E). To assess a more specific end-organ type, we stained for Aβ RA-LTMRs (calbindin-positive, Figure 3B, F), longitudinal lanceolate endings around awl/auchene and guard hair follicles [28]. We found 25% of total calbindin signal overlapped with FM 1–43. In addition to LTMRs, hair follicles receive innervation from circumferential high threshold mechanoreceptive (HTMRs) endings that respond to painful stimuli—such as hair pull—and express the peptidergic nociceptive marker CGRP [30,31]. Although we did sometimes observe FM 1–43-labeled circumferential endings (Figure 3A), a marginal fraction of FM 1–43 labeling was found to colocalize with CGRP (around 2.5%), and less than 1% CGRP signal was positive for FM (Figure 3C, G). One caveat of this colocalization analysis is that FM 1–43 labeling was sometimes spotty or intermittent, likely resulting in an underestimation of actual overlap with more continuous markers like NFH or calbindin. These results indicate that FM 1–43 robustly marks LTMRs in hairy skin.

Terminal Schwann cells tightly envelop lanceolate and circumferential endings at their base [32]. To determine whether FM 1–43 was labeling these cells in addition to neurons, we stained for the Schwann cell marker S100b (Figure 3D, H). Although the interdigitation of Schwann cell protrusions and neuronal endings made the labeling difficult to distinguish, minimal overlap was noted and there were no clearly labeled Schwann cell bodies (Figure 3H). We frequently detected myelin-like labeling of Merkel cell-neurite afferents (Figure

3A), however, it is unclear whether this stems from direct labeling of myelin or a secondary uptake mechanism from association with labeled endings. Our data does indicate that the labeling at the base of hair follicles is neuronal.

Given that we found FM 1–43 uptake occurs at the sites of sensory transduction and that it labels LTMR subtypes (Figure S1I–L, and Figure 3), we next asked whether sensory neuron labeling requires PIEZO2 activity. Gentle touch is almost entirely dependent on PIEZO2 [3,24], so we used this established role to test the *in vivo* activity-dependence of FM 1–43 on PIEZO2 in touch neurons. Longitudinal lanceolate endings respond to hair deflection with exquisite sensitivity [20,21,32], and are sensitive to hair deflection even in the absence of skin indentation [30]. We reasoned that removal of external hair shafts on a patch of leg skin would therefore reduce mechanical activation of these afferents, and hence reduce FM 1–43 loading in this region. Remarkably, labeling of lanceolate endings was significantly reduced in shaved and depilated (with cream) hind-leg skin after 24 h, whereas the hairy regions in the contralateral control leg displayed bright labeling (Figure 4A–C). Investigating the border at the site of depilation revealed lanceolate labeling in the hairy skin that was immediately adjacent to the unlabeled depilated skin (Figure 4A). We expanded our characterization of the labeling patterns in hairy skin by conducting regional analysis of end organ labeling across dorsal skin in the presence or absence of nestlets and wire bar cage tops, which acted as external sources of tactile stimuli normally present in the mouse home cage (Figure 4D–G). In both conditions we observe labeling of lanceolate endings, however, mice housed in cages lacking nestlets and wire bar cage tops accumulated significantly less labeling in back and caudal regions (Figure 4G). The residual labeling could be due to grooming [33], scratching, or interactions with bedding and cage walls. Collectively, these results suggest that FM 1–43 can be used as an indicator of PIEZO2-dependent activity in neurons.

The remarkable labeling specificity of FM 1–43 *in vivo* is surprising because there is precedence for loading through other sensory ion channels *in vitro*. We replicated these results *in vitro* using capsaicin to induce FM 1–43 uptake in TRPV1 expressing cultured HEK cells (Figure S3C–E). Since our *in vivo* labeling is performed in healthy animals where TRPV1 should not be frequently active, we hypothesized that stimulating TRPV1 *in vivo* using capsaicin injection would result in FM dye uptake. To test this, we used *CGRP*$^{cre+}$*;GFP* mice to identify a large portion of TRPV1-expressing neurons (Figure 4H) [34,35]. Mice were first injected with FM 4–64, which avoids spectral overlap with GFP, and 2 h later, we performed subcutaneous hindlimb injections of capsaicin and FastBlue, a retrograde neuronal tracer, to identify DRG neurons innervating the injection site. We filtered for DRGs that were FastBlue/CGRP double positive and assessed for FM 4–64 labeling (Figure 4K). Labeling of nociceptors from the hindlimb was rare (Figure 4I, J), and capsaicin administration failed to produce observable changes in dye uptake relative to the contralateral vehicle (Figure 4K–L). This result was unexpected and further demonstrates the utility of this tool to specifically mark PIEZO2-dependent neuron activity *in vivo*.

To more directly assess whether FM 1–43 labeling depends on PIEZO2 ion channel activity and is not just coinciding with, or downstream of, neuronal activity, we tested dye uptake into cells heterologously expressing human *PIEZO2* in cell culture. For all cell culture

assays related to mechanosensitivity, we use HEK cells engineered to lack endogenous PIEZO1 (HEK P1KO) to avoid potential confounding effects [36]. Two days after transfection with a *PIEZO2* cDNA plasmid, HEK P1KO cells were treated with 10 μM FM 1–43 for 20 minutes followed by washing with Advasep-7 to reduce background signal [37]. Quantification of population fluorescence using flow cytometry revealed that FM 1–43 robustly labeled cells overexpressing PIEZO2 but not cells transfected with control plasmid (Figure 5A–F). We subjected cells to orbital shaking as a simple mechanical stimulation and observed that labeling increased by 49 ± 8%, suggesting stimulus-dependent uptake (Figure 5J). Importantly, fluorescence in control cells was unchanged with orbital shaking (Figure 5A–C), ruling out the possibility that stimulation alone increased background labeling. Notably, dye uptake was observed in *PIEZO2*-overexpressing cells even without shaking. A similar result was observed with TRPV1 overexpression, indicating that some dye permeation can occur even without channel activating stimuli *in vitro* (Figure S3C–E).

To further assess the relationship between FM 1–43 uptake and PIEZO2 channel activity, we transfected $PIEZO2^{R2686H}$ gain-of-function cDNA, a gain of function mutation that has been causally linked to Gordon syndrome and distal arthrogryposis type 5I in human patients [38–40]. This mutation slows current inactivation kinetics, increasing the time constant of inactivation by 435 ± 36% (Figure S4A–D). Consistent with this, we observed a 393 ± 10% increase in signal accumulation in unstimulated $PIEZO2^{R2686H}$ transfected cells over unstimulated *PIEZO2* wild-type (WT) cells. Mechanically stimulated $PIEZO2^{R2686H}$ exhibited a 35 ± 10% increase in fluorescence compared to the unstimulated condition (Figure 5G–J).

As a preliminary attempt to confirm that FM 1–43 entry is attributable to ion channel pore opening, we tested dye uptake in the presence of the non-selective ion channel blocker, Ruthenium Red [41,42]. Concentration-dependent reduction of fluorescence with and without mechanical stimulation was observed with IC_{50} values of 115 ± 27 μM and 135 ± 31 μM, respectively (Figure 5K). This is higher than IC_{50} values (30–50 μM) for inhibiting PIEZO2 currents in sensory neurons [1,43], possibly because FM 1–43 represents cumulative PIEZO2 activity in a field of cells over a longer duration than is typically monitored by electrophysiology. Together, these data reveal a direct relationship between PIEZO2 channel activity and dye uptake.

Previous studies suggest that FM 1–43 can directly permeate mechanotransduction ion channels in DRGs and cochlear hair cells [14,44]. To interrogate channel permeation properties, we conducted a set of electrophysiological recordings on PIEZO1 and PIEZO2 in the presence of FM dye. Cell attached poke (Figure 5. L-O and Figure S5A–E, for PIEZO2 and PIEZO1 respectively), stretch (Figure S5F–I, for PIEZO1), and single channel electrophysiology on cells expressing PIEZO1 (Figure S5J–L) reveal that both PIEZO1 and PIEZO2 are partially inhibited by FM 1–43 in a voltage-dependent manner (Figure 5O, Figure S5D). However, single channel conductance of PIEZO1 is unaltered with FM 1–43 (Figure S5K–L). We used PIEZO1 in these experiments because PIEZO2 does not easily respond to stretch stimuli in patch clamp experiments, and PIEZO1 also takes up FM 1–43 in cell culture (Figure S3A–B, E) in a stimulus-dependent manner. Taken together, it is clear that FM 1–43 inhibits PIEZO currents. Our Ruthenium Red data and the voltage

sensitivity of inhibition implicate pore permeation as an inhibitory mechanism; however, we cannot distinguish with certainty if FM 1–43 induced current reduction results from permeation of this large molecule, or, alternatively, if FM 1–43 is having an allosteric effect on the channel via direct interaction or by altering the plasma membrane (i.e., tension). Further determination of the FM 1–43 internalization mechanism would require thorough electrophysiology and structure-function studies.

The activity dependence of FM 1–43 labeling in awake, behaving mice presents an opportunity to discover novel sensory neurons and physiological processes that rely on PIEZO2. Previously, we found that PIEZO2 was critical for the sensation of bladder fullness and urinary reflexes, and we aimed to use FM 1–43 to identify PIEZO2-positive neurons in the lower urinary tract (LUT) that could mediate these functions [2]. Labeled neuron-like endings were occasionally observed in the bladder muscle and more interior layers (Figure S6A) but were normally difficult to visualize in whole-mounts against high background (Figure S6E–J), in part arising from urothelial labeling (Figure S6H–J). It is possible that urothelial labeling is due to the large amount of vesicular recycling that occurs during bladder stretch [45]. Nerve terminals were often less evident in *HoxB8*$^{Cre+}$;*Piezo2*$^{f/f}$ KO mice compared to WT mice (Figure S6A,B), but even among WT animals, labeling was sparse and varied between animals and bladder regions, making direct comparison difficult.

Nerve endings that could be involved in detecting bladder stretch were difficult to visualize, but mechanosensory neurons associated with the urethra also contribute to urinary reflexes and are not as well studied [46]. Our survey of the LUT with FM 1–43 revealed a novel population of neurons in the male pelvic urethra (Figure 6A). These dense neuronal endings with a tree-like morphology spanned entire lateral urethral region between muscular attachments to the pelvic bone and the curve that begins the penile urethra (Figure 6B–C). These neuron endings failed to label in *HoxB8*$^{Cre+}$;*Piezo2*$^{f/f}$ mice (Figure 6E–F), indicating that, as with other sensory neuronal endings we investigated, their labeling depends on PIEZO2. Morphologically distinct neuronal endings, which looked like simple, free nerve endings, were also observed in the distal urethra of males and females (Figure 6A, Figure S6L). Furthermore, using a dual-labeling strategy with FM 4–64 injected on a short time scale, (also shown in Figure S2D–F), we determined that the “leaves” of the trees are the sites of initial dye entry, and are thus plausible sites of transduction (Figure 6G–I).

In a preliminary effort to elucidate the molecular features of these tree-like urethral neurons, we colocalized FM dye labeling with neuronal markers using whole-mount immunostaining and genetic reporter mice. Despite dense peptidergic innervation of the urinary tract [47,48], these neuron endings were not CGRP-positive (Figure S6K). We also found the tree-like urethral neurons were nearly all NFH positive (Figure 7A–D, I), indicating that these are medium to large diameter neurons, likely originating from DRGs. While the nerve trunks were positive for these structural proteins, immunolabeling did not extend to the endings, so the complex ending morphology was exclusively resolved by the dye. This could explain why this morphology has not been previously described [49] and showcases an advantage of using FM 1–43 for elucidating neuronal localization. Additionally, we confirmed that these structures are still present in *HoxB8*$^{Cre+}$;*Piezo2*$^{f/f}$ KO animals using the

same immunostaining strategy (Figure 7E–H), indicating that the lack of FM dye labeling is due to absence of PIEZO2, and not a developmental loss of these nerve endings.

We next set out to identify the appropriate stimulus sufficient to induce FM 1–43 labeling in urethral neuronal endings. We have previously shown that PIEZO2 is important for micturition reflexes and, given their location, we hypothesized that these neurons would be active during urination. We injected FM 1–43 i.p. in lightly anesthetized mice with a catheter inserted in the bladder as previously described, which allowed us to control fluid filling of the bladder [2]. When we continuously filled the bladder with saline, mice experienced repeated micturition events throughout the duration of the experiment, while sham mice with catheters but no bladder filling did not. Remarkably, urethral neuron labeling was prominent after 1 h of filling, and nearly absent in the unfilled condition (Figure 7J–L). This identifies urination as a relevant stimulus that engages PIEZO2-dependent neuronal activity in urethral neurons.

DISCUSSION

Our results indicate that FM 1–43 can be employed as a specific indicator of PIEZO2 activity in murine somatosensory endings and can be used to identify novel PIEZO2-dependent mechanosensitive processes. The apparent *in vivo* selectivity of FM 1–43 for PIEZO2 is surprising because it has been proposed to permeate various ion channels in cell culture [8]. Other ion channels that are reported to facilitate FM 1–43 permeation in cell culture, such as TRPV1 and P2X, are most active during pain or inflammatory conditions [9,50], but we could not induce labeling in nociceptors even after stimulating TRPV1 with capsaicin injection. This suggests that perhaps the dynamics of channel opening or membrane trafficking are not conducive to labeling through these ion channels *in vivo*.

Given previous findings, FM 1–43 uptake via many sensory ion channels might occur more readily in culture systems than *in vivo*. This difference could arise if FM 1–43 labeling requires high density of cell surface protein expression, which is more easily achieved with overexpression in cell culture. An additional surprise was the preferential uptake of FM 1–43 via PIEZO2 compared to PIEZO1 *in vivo*, as evidenced by a lack of baroreceptor neuron labeling in *Phox2b*^{Cre};*Piezo2*-KO mice (Figure 1E–G) [17,18]. *In vitro*, we also noted that FM 1–43 loads less robustly in HEK cells overexpressing PIEZO1 than those overexpressing PIEZO2 (Figure S3E). However, without surface expression normalization, we cannot rigorously compare labeling efficiency between these heterologously overexpressed ion channels. The broad *in vitro* FM 1–43 labeling could be considered a distinct phenomenon from the specific PIEZO2-dependent somatosensory neuron labeling *in vivo*, and the factors that contribute to this discrepancy are unknown.

It remains unclear if FM 1–43 directly permeates sensory ion channels or if the labeling we observe is downstream of PIEZO2 activity. FM 1–43 has traditionally been used to visualize vesicular recycling associated with synaptic activity because it inserts into lipid membranes. For example, neuronal uptake in motor neurons has been shown to occur through endocytosis [7,51]. However, Meyers et al. (2003) and others found that FM 1–43 uptake in sensory cells did not depend on endocytosis and was brighter and more persistent

than motor neuron uptake, suggesting that it occurs through a distinct mechanism [8,52]. Our work (Figure 5) and previous studies do indicate that FM 1–43 could be capable of permeating mechanosensory ion channels in DRG neurons[14]. If FM 1–43 were competing with other permeant ions during permeation, it might have caused a change in single-channel conductance [53]. The fact that we did not observe a change in conductance (Figure S5K, L) does not rule out permeation: it is possible that either the dwell time of FM 1–43 in the pore is longer than our sampling rate (and thus channels with FM 1–43 appear closed), or that FM 1–43 has a weaker affinity for the pore than other permeant ions, and thus no effect on conductance. It is also possible that this molecule changes membrane stiffness to affect channel gating [54]. Future investigation, including structure-function studies and thorough electrophysiology, will be required to determine the mechanisms of PIEZO2-dependent FM 1–43 uptake.

Nevertheless, our work demonstrates the utility of FM 1–43 as a marker of PIEZO2-dependent neuronal activity. Given other potential mechanisms for cellular uptake, FM 1–43 labeling alone cannot serve as proof of *Piezo2* expression, particularly in cell types that experience frequent endocytic and exocytic activity, such as umbrella cells of the urothelium [45]. This should be a consideration when using FM 1–43 as an *in vivo* labeling tool.

Our finding that the majority of *in vivo* sensory neuron FM 1–43 labeling is dependent on PIEZO2 largely corroborates previous work. For example, Merkel cells label with FM 1–43 injection and express PIEZO2 [5,12]. Interestingly, Moayedi et al. noted that Piezo2-GFP labeling in the oral cavity corresponded to FM 1–43 labeling [11]. Given the many sensory structures that have been shown to label with FM 1–43, we believe that our data can provide additional context to previous work, as labeling could suggest PIEZO2 function. For example, structures observed in bat wings using FM 1–43 might represent PIEZO2-dependent touch receptors [10].

The finding of robust FM 1–43 labeling in species like bats and star-nosed moles highlights an advantage of this technique, as it can be used without specialized genetic tools [10,55]. FM 1–43 can also be used to investigate organs where mechanosensory functions are still poorly understood. In all these cases, confirmation of *Piezo2*-dependence would still be required, but if confirmed, the dye offers a method to strategically design assays to describe the spatial and temporal elements of PIEZO2 activity, as highlighted by our activity-dependence of labeling in hairy skin (Figure 4). Notably, dye injection does not affect animal health or somatosensory behaviors 2 h after administration (Figure S7), despite terminal ending labeling beginning to accumulate by 1.5 h (Figure S1I). Although we did not test behavior at later timepoints, mice appeared normal and healthy. To our knowledge, this is the only example of a tool that allows for permanent localization of the activity of a specific ion channel. Similarly, our data reveal robust FM 1–43 uptake in cell cultures expressing PIEZO2. Taken together, we expect that these dyes will aid researchers in confirming and better defining the many functions of PIEZO2.

As proof of its capability, we use FM 1–43 to pinpoint a unique tree-like nerve ending morphology in the urethra, which appear to be engaged during urination (Figure 7J–L). Further work is needed to fully characterize the origin of these neurons and define their

function in urinary tract physiology, but this finding represents an example of new directions and hypotheses that are enabled by *in vivo* FM 1–43 labeling.

STAR★Methods

RESOURCE AVAILABILITY

Lead contact—Further information and requests for resources and reagents should be directed to the lead contact, Kara Marshall (kara.marshall@bcm.edu).

Materials availability—Plasmids generated in this study are available upon request.

Data and code availability

- Microscopy and all other data reported in this paper will be shared by the lead contact upon request.
- This paper does not report original code.
- All data and any additional information required to reanalyze the data reported in this paper is available from the lead contact upon request.

EXPERIMENTAL MODEL AND STUDY PARTICIPANT DETAILS

Mice—All animal procedures were approved by the Institutional Animal Care and Use Committees of The Scripps Research Institute (TSRI). All animals were housed in the same vivarium conditions at a constant temperature of 22 °C, and humidity between 30% and 80% (not controlled), with a 12 h light/dark cycle. Age-matched knockout and wildtype littermates were tested at the same age in each experiment, ranging from 10–24 weeks. Littermates were randomly assigned to experimental groups. The sex of mice used is reported in figure legends. Animals were kept group housed, unless otherwise specified in the relevant methods section. All Piezo2^{cre} mice were maintained on C57BL/6 background. The *HoxB8^{Cre};Piezo$^{f/f}$* and *Phox2b^{Cre};Piezo2$^{f/f}$* mouse lines have been previously described [4,6]. CGRP-GFP mouse line has been previously described[35], and was a generous gift from Mark Zylka. Genotyping was performed using guidelines from Jackson Laboratory. C57BL/6J adult mice were used for all experiments if not otherwise defined in the text. For *in vivo* FM labeling experiments everywhere but the urethra, male and female mice were used interchangeably. However, we did not perform an analysis of the influence of sex on experimental outcome because labeling patterns appeared consistent between male and female mice in all organs except the urethra.

Cell Lines—HEK293T cells CRISPR-engineered to lack endogenous expression of Piezo1 (HEK-P1KO cells, female), were previously generated in Dr. Ardem Patapoutian's laboratory and are available on ATCC (Cat.# CRL-3519), were used for cell culture flow cytometry experiments and electrophysiology. Cells were cultured in DMEM containing 10% FBS and 100 U/mL penicillin/streptomycin (Thermo Fisher). Cells were maintained at 37 °C and 5% CO2.

Neuro2A cells CRISPR-engineered to lack endogenous expression of Piezo1 (Neuro2A-P1ko; a gift of Gary Lewin [56]) were used for electrophysiology and were cultured at 37°C and 5% CO_2 in Minimum Essential Medium (Thermo Fisher) supplemented with 0.1 mM non-essential amino acids, 1 mM pyruvate, 10% FBS (Clontech), 50 U/mL penicillin, and 50 mg/mL streptomycin (Life Technologies). Cells, male, were STR authenticated by ATCC and tested negative in-house for mycoplasma via PCR (ATCC #30–1012K).

METHOD DETAILS

Cloning—The full-length sequence of human PIEZO2 transcript variant 2 (10520bp) was codon-optimized using the Thermo Fisher Gene Art Codon Optimization tool. G-blocks for this sequence were then generated by Azenta Life Sciences and were assembled using Gibson Assemble master mix (NEB: E2611) into a mammalian expression vector modified from pCDNA3.1 to contain a T2A self-cleaving peptide followed by an in-frame blue fluorescent protein (BFP) and a woodchuck hepatitis virus post-transcriptional regulatory element (WPRE). The final construct yielded was pCDNA3.1-*PIEZO2*-T2A-BFP-WPRE (“*PIEZO2”).*

To generate the human *PIEZO2*^{R2686H} gain-of-function construct, the above sequence was modified using Q5 site-directed mutagenesis (E0554) directed at amino acid 2686 to substitute histidine for arginine, yielding pCDNA3.1-*PIEZO2_R2686H*-T2A-BFP-WPRE (“*PIEZO2*^{R2686H}*)*, full sequence in Supplemental Table 3. For all full plasmid sequences of generated constructs, see Tables S1–4.

Cell culture and transfection—The HEK P1KO cell line was maintained in DMEM (4.5 mg/ml glucose) with 10% FBS and pen/strep antibiotics for all transfection experiments. Prior to transfection, cells were plated on Matrigel (Corning: 354234), 75–90 μg/mL, coated Falcon Polystyrene 6-well tissue culture plates. When cells reached 50–70% confluency, cDNA was transfected into cells using PEI MAX at 1 μg/μL. 2 μg of DNA was transfected per well employing a ratio of 3:1 PEI (μg) to DNA (μg). Cells were transfected two days prior to FM 1–43 labeling experiments. Cells from control condition were transfected with an empty vector containing BFP.

FM 1–43 fluorescence-based cell culture assay—For cell culture labeling experiments, FM 1–43FX (Invitrogen: 35355) was resuspended at 10 μM in Hanks Buffered Saline Solution (HBSS, 10 mM HEPES, pH7.4). ADVASEP-7 (Biotium) was also resuspended at 500 μM in HBSS. Two days after transfection, cells were washed with HBSS and 10 μM FM 1–43 was applied to cells. For stimulated condition, cells were placed on an orbital shaker (setting 6–7 out of 10), while unstimulated cells were left on a benchtop, both at room temperature. After 20 minutes, cells were washed twice with 500 μM ADVASEP-7, 3 minutes per wash with orbital shaking.

For FM 1–43 labeling inhibition experiments, Ruthenium Red (RR, Sigma: R2751) was resuspended in HBSS at stated concentrations (Figure 5K). Cells were preincubated with RR for 10 minutes and contained RR at the indicated concentrations during FM 1–43 labeling. In addition to two ADVASEP-7 washes, cells were washed twice more with HBSS to remove residual RR. To generate Ruthenium Red IC50 values in Prism

(Graphpad), a nonlinear regression model using the ‘Dose-response – Inhibition’ ([Inhibitor] vs. normalized response) equation was fit to the data assuming a standard slope (Hill Slope = −1.0).

Electrophysiology

Whole cell poke: Mechanically activated currents from HEK P1KO cells 2 days after transfection were recorded in whole-cell patch clamp mode using a MultiClamp700A amplifier and DigiData1550 (Molecular Devices) and stored directly and digitized online using pClamp software (version 10.7). Currents were sampled at 20 kHz and filtered at 2 kHz. Recording electrodes had a resistance of 2 to 5 megohms when filled with CsCl-based intracellular solution: 133 mM CsCl, 1 mM $CaCl_2$, 1 mM $MgCl_2$, 10 mM HEPES (pH with CsOH), 5 mM EGTA, 4 mM Mg-ATP (adenosine triphosphate), and 0.5 Na-GTP (guanosine triphosphate). Extracellular bath solution was composed of 133 mM NaCl, 3 mM KCl, 2.5 mM $CaCl_2$, 1 mM $MgCl_2$, 10 mM HEPES (pH 7.3 with NaOH), and 10 mM glucose. Mechanical stimulation was achieved using a fire-polished glass pipette (tip diameter, 3 to 4 μm) positioned at an angle of 80° relative to the cell being recorded. Displacement of the probe toward the cell was driven by Clampex-controlled piezoelectric crystal microstage (E625 LVPZT Controller/Amplifier; Physik Instrumente). The probe had a velocity of 1 μm ms−1 during the ramp phase of the command for forward movement, and the stimulus was applied for a duration of 125 ms. For each cell, a series of mechanical steps in 1 μm increments was applied every 10 s.

Inhibition at −80 and +80 mV (percent of peak response at the same displacement above threshold; threshold + 3 or 4 μm) was determined using two protocols which provide similar results. The first evoked stimulus intensity-dependent increases in MA currents (families) at both potentials (10 sec interstimulus interval). 1 μm increments were applied to enable acquisition in FM 1–43fx at both −80 mV and +80 mV at least once to observe inhibition before washout by gravity feed.

A second protocol was used to confirm the results acquired from the first protocol, because it often required at least 3–5 minutes per family and cells sometimes became leaky in the FM 1–43fx. After families were acquired, a single stimulus at 2 or 3 μm above threshold was applied at −80 mV followed by that same stimulus at +80 mV after a 10 sec wait. This was repeated again after 10 sec, in multiple rounds. Directly comparing responses at each potential within 10 sec confirmed the voltage dependence of inhibition. Families were again taken after inhibition was observed and similar results obtained. Stimulus dependent mechanically activated (poke) currents were acquired under control conditions. Displacements are shown for mechanically activated currents in all figure panels.

Cell attached: Neuro2A cells were transiently transfected 40–48 h prior to recording with 4 μg of human Piezo1-pIRES2-EGFP in 6-well plates using Lipofectamine 2000 (Thermo Fisher Scientific) and replated onto poly-L-lysine and laminin coated coverslips 16–24 h before recording.

Cell-attached electrophysiological recordings were performed at room temperature using an EPC10 amplifier and Patchmaster software (HEKA Elektronik). Data were sampled at 10

kHz and filtered at 2.9 kHz; single-channel measurements were additionally digitally filtered offline at 1 kHz prior to analysis. The bath solution used to zero the membrane potential was (in mM): 155 KCl, 3 $MgCl_2$, 5 EGTA, 10 HEPES, pH 7.35 with NaOH. Borosilicate glass pipettes (1.5 OD, 0.85 ID, Sutter Instrument Company) were filled with pipette buffer solution (in mM): 150 NaCl, 5 KCl, 2 $CaCl_2$, 1 $MgCl_2$, 10 HEPES, pH 7.3 with NaOH. Negative pressure was applied through the patch pipette with an amplifier-controlled high-speed pressure clamp system (HSPC-1; ALA Scientific Instruments).

All data were analyzed using Igor Pro 8.02 (Wavemetrics). Peak currents for pressure-response curves were measured following baseline subtraction during 50–200 ms of the mean current immediately prior to the pressure stimulus.

Single channel current amplitudes were calculated by generating all-points histograms with binning determined using the Freedman-Diaconis method and an optimal bin width of $2*IQR(x)/N^{1/3}$, where IQR is the interquartile distance, N is the number of observations, and the bins are evenly distributed between the minimum and maximum values. Histograms were then fit with a double-Gaussian equation of the form,

$$y = y_0 + A_1 * exp - \left(\frac{x - x_1}{w_1}\right)^2 + A_2 * exp - \left(\frac{x - x_2}{w_2}\right)^2$$

where y_0 is the baseline current, A_1 and A_2 are the peak amplitudes, x_1 and x_2 are the centers of the fits, and w_1 and w_2 their respective widths. The difference between x_1 and x_2 reflects the difference between mean current in the open and closed state and was used to calculate single channel currents. 1–5 openings per patch were analyzed at each voltage. For control solution, spontaneous openings (in the absence of pressure) were analyzed. For FM 1–43fx, −10 to −30 mmHg was used to elicit openings, owing to lower spontaneous activity in this condition. Slope was calculated from a weighted fit of single-channel current as a function of voltage, taking into account the standard deviation of the current at each potential.

Fluorescence activated cell sorting—For quantitative fluorescence analysis of FM 1–43 labeled HEK cells, cells were dissociated with 0.05% Trypsin-EDTA (Gibco: 25300054), washed once in FACS buffer (PBS supplemented with 2% FBS and 1 mM EDTA), resuspended in FACS buffer at 100K cells per mL, and strained into a 5 mL polystyrene Round-Bottom tube (Corning: 352235). Samples were then analyzed using the ACEA NovoCyte 3000 with NovoSampler Pro. Cells transfected with *PIEZO2* and *PIEZO2-R2686H* cDNA were gated on BFP, and subsequently FITC-A population mean fluorescent intensities were used as a fluorescent readout of FM 1–43 labeling. Data were analyzed using FlowJo (BD). Mean fluorescence values from ‘Control’ were interpreted as background labeling and were subtracted from mean fluorescence values of the experimental conditions. Remaining values were then normalized to the ‘PIEZO2 WT Unstimulated’ condition which operated as an internal control for comparing results between separate experiments. For Figure 5 and Figure S3, three FACS experiments were run per group with 3 biological replicates per experiment unless otherwise specified. A minimum of 50k cells were analyzed per individually plotted point.

FM styryl dye labeling and tissue collection—Unless otherwise stated, mice were injected intraperitoneally with FM 1–43FX (Invitrogen: F35355) or FM 4–64FX (Invitrogen: F34653), at a dose of 1.12 mg/kg of body weight from stocks made up in PBS. At time post-injection time point indicated in the text, mice were perfused with PBS followed by 4% PFA. Tissues were subsequently dissected and drop fixed for a minimum of 1 h (smaller tissues) at 4°C and up to 24 h (larger tissues) at 4°C prior to imaging or immunostaining.

For urethra sectioning, tissue was fixed in 4% PFA for 24 h, embedded in Tissue Tek OCT (Sakura: 4583), and frozen. Using the cryostat, 30 μm cross sections throughout the pelvic urethra were generated onto Superfrost Plus microscope slides (Fisher: 12–550-15). Sections were then washed with PBS to remove OCT before mounting or staining.

Cystometry—C57BL/6J male mice were anesthetized by isoflurane (3% induction, 1.1–1.4% maintenance, Kent Scientific SomnoSuite) and the bladder was catheterized and connected to saline lines, as described previously [2]. Saline lines were connected to a pressure sensor (Biopac: RX104A-MRI) which connected via pressure transducer (TSD104A) to an MP160 Biopac system amplifier (DA100C). After catheter lines were inserted, FM 1–43 was applied in the abdominal cavity to simulate an i.p. injection. Using a syringe pump, the bladder was continuously filled at 30 μl min^{-1} to induce urination events in the ‘filled’ condition. Mice in ‘unfilled’ condition were prepared in the same manner but bladders were taken to a low-fill state before the FM 1–43 application, and they did not receive continuous saline bladder filling. Filling (or no filling) continued for 60 min, after which mice were euthanized, and perfused with PBS and 4% PFA. The urethra was then collected, drop fixed in 4% PFA for 1 h, and imaged in a whole mount preparation.

Immunohistochemistry—Skin and pelvic urethra whole-mount immunostaining was performed as previously described for skin [59]. Tissues were collected from 8–12 week-old wildtype C57BL/6J mice after perfusion with 4% PFA. Tissues were fixed overnight in 4% PFA, washed 3 times in PBS, and washed for 5 h in approximately 40 mL of PBS with 0.1% TritonX-100 (PBST), changing the PBSt every hour. Tissues were then placed in blocking solution consisting of 5% normal goat serum (NGS), 20% DMSO, 75% PBSt, along with primary antibodies. The primary antibodies used on skin and/or urethra were chicken anti-neurofilament heavy chain (NFH) (1:500 dilution, Abcam: ab4680), rabbit anti-Calbindin D-28k (Swant AG, Burgdorf, Switzerland, Cat. CB-38a, 1:750), rabbit anti-CGRP (Abcam, Cat. ab47027, 1:200), rabbit anti-S100b (Abcam, Cat. Ab52642, 1:500) and rabbit anti-beta III tubulin (1:500 dilution, Abcam: ab18207). Tissue was incubated for 4 days at 4°C on a rocker. Next the samples were washed in a large volume of PBSt for 5 h, changing PBSt every hour. Samples were then placed in blocking solution containing secondary antibodies. The secondary antibodies used were goat anti-chicken AlexaFluor 647 (Invitrogen A21449) and donkey anti-rabbit AlexaFluor 594 (A21207), all diluted at 1:500. Tissues were incubated for 2 days at 4°C on a rocker, with final washes in a PBSt for at least 5 h, with frequent PBSt changes. Samples were then blotted dry on a clean Kimwipe (Kimtech) and were mounted onto Superfrost Plus microscope slides.

For DRG immunostaining, 5–10 DRGs were harvested from each spinal region (cervical, thoracic, or lumbar). Tissues were fixed in 4% paraformaldehyde (PFA) for 1 h on ice,

cryoprotected in 30% sucrose overnight at 4°C, then frozen in O.C.T. (Fisher Healthcare, TX, USA, Cat. 23–730-571) and sectioned at a thickness of 25 μm. Cryosectioned DRGs were rinsed with PBS for 5 min. to remove O.C.T., permeabilized and blocked in 5% normal goat or donkey serum in 0.3% PBS-Triton X-100 (PBST) for 1–2h at room temperature, then labelled with one of the following primary antibodies diluted in 0.3% PBST overnight at 4°C: chicken anti-TH (Abcam, Cat. ab76442, 1:500), goat anti-TRKA (Biotechne R&D Systems, Cat. AF1056-SP, 1:500), chicken anti-NFH (Abcam, Cat. ab4680, 1:1000), rabbit anti-Calbindin D-28k (Swant AG, Burgdorf, Switzerland, Cat. CB-38a, 1:750), or mouse anti-CGRP (Abcam, Cat. ab81887, 1:200). Tissue sections were then briefly washed in PBS, then incubated for 1h at RT with the appropriate secondary antibody, diluted 1:1000 in 0.3% PBST: donkey anti-goat IgG (H+L) cross-adsorbed secondary antibody, Alexa Fluor™ 647 (Thermo Fisher Scientific, A-21447), goat anti-chicken IgY H&L Alexa Fluor™ 647 (Abcam, ab150171), goat anti-rabbit IgG H&L Alexa Fluor™ 647 pre-adsorbed (Abcam, ab150083), or goat anti-mouse IgG H&L Alexa Fluor™ 405 (Abcam, A31552). Isolectin IB_4 staining was combined with CGRP staining during the secondary antibody incubation step using 5 μg/mL Isolectin GS-IB4 from *Griffonia simplicifolia*, Alexa Fluor™ 647 Conjugate (Thermo Fisher Scientific, Cat. I32450). Finally, samples were washed 5 × 10 min. in PBS, mounted with SlowFade™ Gold anti-fade mountant with/without DAPI (Thermo Fisher Scientific, S36939), and imaged on a Zeiss LSM880 with Airyscan FAST confocal microscope equipped with 20X, 0.8 numerical aperture (NA) objective lens. Acquisition settings were matched between mice for each spinal region per marker.

Capsaicin and FastBlue tracer injection—$CGRP^{cre+}$;GFP female (N=1) and male (N=2) mice were anesthetized by isoflurane (3% induction, 2.0–2.5% maintenance). 2 h prior to capsaicin injection, mice were given i.p FM 4–64. Next mice were injected with 0.5 μg/μL (0.05%) capsaicin (Sigma-Aldrich M2028) made up in 0.1% PBS, 0.5% Tween-80, 10% EtOH, and 1.25% FastBlue tracer (Polysciences 17740–1) vehicle solution. Capsaicin was administered at 0.5 μg per g of animal weight, and the resulting volume was split equally between three subcutaneous injections (Figure 4H) using a Hamilton's syringe, totaling 17–21 μL. Contralaterally, mice were injected with vehicle control. 3 days later mice were euthanized and L4-L6 DRGs were collected, fix o/n in 4% PFA, and image on a confocal microscope.

Lectin labeling of DRG vasculature—Two hours after FM 1–43FX injection, mice were terminally anesthetized with isoflurane, and transcardially perfused with 10 mL of 1X PBS. Immediately following this, 10 mL of 1X PBS containing 10 μg/mL of Lycopersicon esculentum (Tomato) Lectin (LEL, TL), DyLight 649 (Invitrogen Cat.# L32472), was perfused into the mouse, and allowed to stain for 2 minutes before a final perfusion with 10 mL of 4% PFA. DRGs were then dissected, fixed in 4% PFA for 1 hour, and imaged on a confocal microscope.

Confocal imaging—Prior to imaging, tissue was covered in Fluoromount G mounting medium with DAPI (Thermo: 00–4959-52) and number 1.5 coverglass was placed over the tissue. All confocal settings for a given experiment were imaged on the same microscope with identical settings for direct comparison of fluorescent brightness. Tissues were imaged

on a Nikon C2 confocal mounted on an upright 90i microscope or an inverted NikonA1 confocal. For the Nikon C2, the following objectives were used: 10x PlanApo 0.45 Dry, 20X PlanApo, 0.8 Dry, 40X PlanFluor 1.3 Oil, and 60x PlanApo VC1.4 Oil. Laser lines used include 408nm, 488nm, 561nm and 637nm. Nikon C2 emission filters include 450/40nm, 514/30nm, and 585/65nm. For the NikonA1, the following objectives were used: 10x PlanApo 0.45. Laser lines included 405nm, 488nm, 561nm, and 638nm. Nikon A1 emission filters include 450/25nm, 525/25nm, 600/25nm, and 685/35nm.

Skin samples from Figure 4A–C were imaged under 20X magnification for quantification of FM 1–43 fluorescence signal: 405 nm laser set to 5% transmission strength, 650 master gain, 0 digital offset; 488 nm laser set to 2% transmission strength, 620 master gain, 100 digital offset; 25–30 μm stacks collected at 0.9–1 μm increments and 0.208 μm/pixel resolution. The border between hairy and shaved skin was imaged under 5X magnification: 488 nm laser set to 7% transmission strength, 725 master gain, 1.00 digital offset; 140 μm stack collected at 10 μm increments and 0.830 μm/pixel resolution. Emission filters: 419–480 nm for 405 nm laser; 526–625 nm for 488 nm laser. Example images represent maximum intensity projections. The sections were imaged in LSM 880 at 10x magnification using 488 nm and 405 nm laser to visualize the FM 1–43 labelled lanceolate endings and the hair shafts, respectively. The control and the experimental groups were imaged with the same settings.

Image quantification

DRG: Images were analyzed in FIJI (ImageJ) or Imaris (version 9.9.1. Figure 3 and Figure 4I–L). For images of whole-mount DRGs, nodose ganglia, aorta, a region of interest was drawn on each image, and mean brightness was measured. For DRGs from Figure 1A–B, an average background pixel brightness value was measured by taking mean intensity from an area without tissue from 36 images from both genotypes. This background value was subtracted from all brightness values. Tissue filled the area for some images, which is why an average background value was used. C4-C6 has only 2 WT animals per group, so cervical levels were not statistically compared, and cervical regions are not expected to differ as *HoxB8*^{Cre} should not be active there. Thoracic and Lumbar regions have tissue from 3–4 mice per group. An average mean intensity value for all thoracic or all lumbar DRG images was calculated per animal, and these regional averages were compared between WT and KO. For aorta (Figure 1E–G), mean intensity measurements were normalized to ROI area.

To quantify the percentage of FM 1–43 positive DRG cell bodies which were also positive for each cell marker in sectioned DRGs (Figure 2), a region of interest (ROI) was drawn around individual cells which are FM 1–43 positive based on FM 1–43 channel view only (i.e., cell marker channel was hidden to eliminate bias). Only cells with visible nuclei were counted. Next, mean brightness was measured for ROIs on cell marker channel. Cells with mean intensities above a set threshold, matched for each spinal region across animals per marker, were counted as double-positive. For each cell marker, 3–5 individual DRGs per region (cervical, thoracic, lumbar) per animal were analyzed for a total of 9–15 DRGs. In 1 out of 3 animals, only thoracic and lumbar DRGs were analyzed. To quantify the proportion of cell marker-positive cells which are also FM 1–43 positive, the same approach

was followed with the ROI selection being performed on cell marker channel only (i.e., FM 1–43 channel hidden). Total number of cells analyzed per animal per marker ranged from 78 to 703, depending on marker abundance.

For DRG FM 4–64 and GFP colocalization in Figure 4I–J, Imaris Surfaces tool was used on z-stack images of lumbar DRGs to create 3D surface-based objects of cell bodies from each channel. In brief, surfaces were thresholded based on absolute intensity and a quality filter was applied to the resulting volumes. The shortest-distance calculation was used to determine the total number of non-overlapping objects (if a distance value was <0). The number of non-overlapping objects was then divided by the total number of objects identified for each respective channels, and the resulting number was converted to a percent. For Figure 4K–L, the Surface-Surface colocalization was used to assess for double-positive GFP (CGRP-positive) and FastBlue (hindlimb traced DRGs) objects. CGRP+/FastBlue+ objects were then colocalized with surfaces constructed from the FM 4–64 channel. The resulting triple-positive (CGRP+/FastBlue+/FM 4–64+) objects were manually filtered to rule out false-positives. The number of triple-positive objects was then divided by the total number of FastBlue+/CGRP+ and were converted to a percent (Figure 4L).

Hairy Skin: For hair follicle labeling quantification in Figure 1L, 7–10 images of whole mount hairy skin were taken from each mouse. Follicles were identified by blue autofluorescence, and those labeled with FM 1–43 were counted manually. For Figure 4A–C, on Day 1, animals were anesthetized using isoflurane and the skin over the dorsal thigh surface of one hind leg was de-haired with depilatory cream. Animals recovered overnight. On Day 2, animals received a single i.p. injection of FM 1–43 dye (10 μL/g at 200 μM). 16 h post-injection, animals were perfused with ice cold PBS then 4% PFA. Equivalent skin samples from the dorsal thigh surface of each hind leg, 1 ‘Hairy’ and 1 ‘Shaved’ sample per animal, were drop fixed in 4% PFA for a minimum of 1 h at 4 °C prior to whole mounting and imaging.

For hairy skin immunostaining FM 1–43 colocalization, wholemount z-stack images were analyzed using the Imaris Coloc tool. Briefly, thresholds were established for FM 1–43 and marker channels, and were applied to all images. The ‘% volume above threshold’ statistic was then generated for each channel, 5–7 images analyzed per mouse, N=3 mice per marker.

For hairy skin touch stimuli experiments, animals received an i.p. injection of FM 1–43 and were singly housed for 24 hours prior to harvesting their skin. The experimental group had access to tactile stimuli in the form of low hanging cage bar, which was 3.5 cm above the ground of the cage. It allowed a gap of 0.5 – 2.5 cm based on the varied thickness of the bedding on the ground. The experimental group also had access to an enrichment nestlet. The control group did not have access to either the low hanging wire bar or the nestlet. The animals were euthanized and perfused with cold PBS followed by 4% PFA. The dorsal skin hair was shaved with a trimmer and Nair depilatory cream was applied on shaved skin for 30 seconds before wiping it with ethanol. The dorsal skin was then peeled, and the dermal fat was scrapped off. The dorsal skin was stuck on an index card with dermal side facing the card to retain its shaped and drop fixed in PFA for 3 days. The skin was then peeled off the index card and kept in clearing solution for one day prior to imaging. Whole skin images

were taken using the AxioZoom Widefield Scope at 1600ms exposure using 25x lens, and the tiles were stitched together to get the whole image of the skin. The skin was then cut into 10 regions and mounted on superfrost slides with the clearing solution for confocal imaging. Confocal images were used for quantification of dye uptake by the lanceolate endings. The dorsal skin of the animal was divided in four regions for quantification, and 10–20 images were taken spanning each region. The total pixel number above a set threshold was counted for all the images taken in these regions, to give a region-wise comparison of the dorsal skin in the experimental and the control group. Mean values from all the images from each region of each animal were compared. Threshold was chosen based on the average value calculated from 90 images that allowed lanceolate labeling to be counted without including background follicle labeling. Images from both conditions were assessed to choose the appropriate threshold, and once chosen, the same threshold value was used to quantify all images.

Urethra: For quantification of urethra images, images were taken evenly across the pelvic urethra region from each mouse to ensure a large portion of this region was captured even when no neuronal structures were visible. A threshold value was chosen from areas without labeling in order to reduce autofluorescence, and the same threshold was applied to all images in a given experiment. The entire image was filled by tissue, and the thresholded mean brightness of the entire image was measured. For Figure 6F, 4–6 images were taken per mouse. For Figure 7L 3–5 images were taken per mouse. The mean of all images was then taken for each animal, and these animal averages were compared between groups.

For quantification of NFH+ endings in the urethra (Figure 7I), max intensity projections from z-stacks of immunostained and FM 1–43 (24 h) labeled tissue were generated. Individual FM 1–43 labeled endings were identified manually, followed by binary determination of NFH+ innervation at their respective terminal branches. 4–5 images were analyzed per animal.

Behavior

Tape on back: Two hours after injection of FM 1–43 animal were placed in a clear acrylic, cylindrical container and allowed to acclimate to their surroundings for at least 15 minutes. A one inch piece of lab tape is placed in the lower, caudal region of the animals back, about an inch above the base of the tail. The tape remains on the back of the animal for 5 minutes and the number of bouts attempted to remove the tape were recorded. A bout is considered any attempt to turn around and/or remove the tape, “wet-dog” shakes, and scratching at the tape with the hind paw.

Up/down Von Frey: Animals were acclimated in Von Frey chambers for a duration of 1 h for two days. On the third day animals were acclimated in Von Frey chambers for 1 h and baseline up/down Von Frey measurements were taken. The 50% mechanical threshold was measured with Von Frey filaments (0.07, 0.16, 0.4, 0.6, 1.0, 1.4, 2.0, 4.0 and 6.0 g) using the up-down method [60], On day four animals were injected with 1.12 mg/kg of FM 1–43 intraperitoneally and returned to their cages for one hour. The animals were then put into Von Frey chambers and acclimated for 1 h and the 50% threshold was measured again.

Rotarod: Rotarod balancing requires a variety of proprioceptive, vestibular, and fine-tuned motor abilities as well as motor learning capabilities (Carter et al., 2001). An AccuRotor rotarod apparatus (Omnitech Electronics, Inc., Columbus, OH) was used in these studies. A protocol was used whereby the rod starts in a stationary state and then begins to rotate with a constant acceleration of 10 rpm. When the mice are incapable of staying on the moving rod, they fall 38cm into a sanichip bedding filled chamber, breaking a photobeam in the process. The time of fall (sec) is recorded by computer. The mice were trained in 3 sets of 3 consecutive trials on day 1. On day 2, the mice were retested in 3 consecutive trials, injected with FM 1–43, and then tested in an additional 3 trials 2 hr post injection.

QUANTIFICATION AND STATISTICAL ANALYSIS

Graphing and statistical analysis was performed in Prism (GraphPad 9.2.0). Groups were compared using appropriate statistical tests as stated in the figure legends and methods. Welch's two-tailed t-test was used for single comparisons between wildtype and KO groups. Unpaired two-tailed t-test was used in cell culture flow cytometry experiments where variance could be assumed to be equal. The paired two-tailed t-test was used when comparing from within a single subject, such as an experimental condition vs contralateral control, or if before and after comparisons were made on a single subject, such as electrophysiological recordings of a cell, before and after treatment. P-value > 0.05 shown as 'ns', ≤ 0.05 shown as '*', ≤ 0.01 shown as '**', ≤ 0.001 shown as '***', and ≤ 0.0001 shown as '****'. For animal experiments, 'N' refers to the number of animals per condition, unless otherwise specified in the figure legends.

ADDITIONAL RESOURCES

Figure design and visualization—Figures and graphical illustrations were designed with Adobe Illustrator and Biorender (Biorender.com).

Supplementary Material

Refer to Web version on PubMed Central for supplementary material.

ACKNOWLEDGEMENTS

The authors thank the Patapoutian lab for many helpful discussions, in particular A. Koster, E. Lumpkin for early discussions, R. Hill, L. Drew and A. Chesler for comments on the manuscript. This project was supported by the Optical Imaging & Vital Microscopy (OiVM) Core at the Baylor College of Medicine, with the expert assistance of Jason Kirk, as well as the Nikon Center of Excellence at Scripps Research with the expert assistance of K. Spencer, and the Animal Behavior Core at Scripps Research with the expert assistance of Amanda Roberts. This work was supported by the Howard Hughes Medical Institute; the NIH grants R35 NS105067 to A.P., F32 DK121494 and K99 DK128621 and the McNair Medical Institute, Robert and Janice McNair Family Foundation to K.L.M.

Inclusion and Diversity

We support inclusive, diverse, and equitable conduct of research.

REFERENCES

1. Coste B, Mathur J, Schmidt M, Earley TJ, Ranade S, Petrus MJ, Dubin AE, and Patapoutian A (2010). Piezo1 and Piezo2 are essential components of distinct mechanically activated cation channels. Science 330, 55–60. 10.1126/science.1193270. [PubMed: 20813920]
2. Marshall KL, Saade D, Ghitani N, Coombs AM, Szczot M, Keller J, Ogata T, Daou I, Stowers LT, Bonnemann CG, et al. (2020). PIEZO2 in sensory neurons and urothelial cells coordinates urination. Nature 588, 290–295. 10.1038/s41586-020-2830-7. [PubMed: 33057202]
3. Ranade SS, Woo SH, Dubin AE, Moshourab RA, Wetzel C, Petrus M, Mathur J, Begay V, Coste B, Mainquist J, et al. (2014). Piezo2 is the major transducer of mechanical forces for touch sensation in mice. Nature 516, 121–125. 10.1038/nature13980. [PubMed: 25471886]
4. Woo SH, Lukacs V, de Nooij JC, Zaytseva D, Criddle CR, Francisco A, Jessell TM, Wilkinson KA, and Patapoutian A (2015). Piezo2 is the principal mechanotransduction channel for proprioception. Nat Neurosci 18, 1756–1762. 10.1038/nn.4162. [PubMed: 26551544]
5. Woo SH, Ranade S, Weyer AD, Dubin AE, Baba Y, Qiu Z, Petrus M, Miyamoto T, Reddy K, Lumpkin EA, et al. (2014). Piezo2 is required for Merkel-cell mechanotransduction. Nature 509, 622–626. 10.1038/nature13251. [PubMed: 24717433]
6. Zeng WZ, Marshall KL, Min S, Daou I, Chapleau MW, Abboud FM, Liberles SD, and Patapoutian A (2018). PIEZOs mediate neuronal sensing of blood pressure and the baroreceptor reflex. Science 362, 464–467. 10.1126/science.aau6324. [PubMed: 30361375]
7. Betz WJ, Mao F, and Smith CB (1996). Imaging exocytosis and endocytosis. Curr Opin Neurobiol 6, 365–371. Doi 10.1016/S0959-4388(96)80121-8. [PubMed: 8794083]
8. Meyers JR, MacDonald RB, Duggan A, Lenzi D, Standaert DG, Corwin JT, and Corey DP (2003). Lighting up the senses: FM1–43 loading of sensory cells through nonselective ion channels. J Neurosci 23, 4054–4065. [PubMed: 12764092]
9. Karashima Y, Prenen J, Talavera K, Janssens A, Voets T, and Nilius B (2010). Agonist-induced changes in Ca(2+) permeation through the nociceptor cation channel TRPA1. Biophys J 98, 773–783. 10.1016/j.bpj.2009.11.007. [PubMed: 20197030]
10. Marshall KL, Chadha M, deSouza LA, Sterbing-D'Angelo SJ, Moss CF, and Lumpkin EA (2015). Somatosensory substrates of flight control in bats. Cell Rep 11, 851–858. 10.1016/j.celrep.2015.04.001. [PubMed: 25937277]
11. Moayedi Y, Duenas-Bianchi LF, and Lumpkin EA (2018). Somatosensory innervation of the oral mucosa of adult and aging mice. Sci Rep 8, 9975. 10.1038/s41598-018-28195-2. [PubMed: 29967482]
12. Maksimovic S, Nakatani M, Baba Y, Nelson AM, Marshall KL, Wellnitz SA, Firozi P, Woo SH, Ranade S, Patapoutian A, and Lumpkin EA (2014). Epidermal Merkel cells are mechanosensory cells that tune mammalian touch receptors. Nature 509, 617–621. 10.1038/nature13250. [PubMed: 24717432]
13. Majumder P, Moore PA, Richardson GP, and Gale JE (2017). Protecting Mammalian Hair Cells from Aminoglycoside-Toxicity: Assessing Phenoxybenzamine's Potential. Front Cell Neurosci 11, 94. 10.3389/fncel.2017.00094. [PubMed: 28503132]
14. Drew LJ, and Wood JN (2007). FM1–43 is a permeant blocker of mechanosensitive ion channels in sensory neurons and inhibits behavioural responses to mechanical stimuli. Mol Pain 3, 1. 10.1186/1744-8069-3-1. [PubMed: 17207285]
15. Witschi R, Johansson T, Morscher G, Scheurer L, Deschamps J, and Zeilhofer HU (2010). Hoxb8-Cre mice: A tool for brain-sparing conditional gene deletion. Genesis 48, 596–602. 10.1002/dvg.20656. [PubMed: 20658520]
16. Murthy SE, Loud MC, Daou I, Marshall KL, Schwaller F, Kuhnemund J, Francisco AG, Keenan WT, Dubin AE, Lewin GR, and Patapoutian A (2018). The mechanosensitive ion channel Piezo2 mediates sensitivity to mechanical pain in mice. Sci Transl Med 10. 10.1126/scitranslmed.aat9897.
17. Min S, Chang RB, Prescott SL, Beeler B, Joshi NR, Strochlic DE, and Liberles SD (2019). Arterial Baroreceptors Sense Blood Pressure through Decorated Aortic Claws. Cell Rep 29, 2192–2201 e2193. 10.1016/j.celrep.2019.10.040. [PubMed: 31747594]

18. Elsaafien K, Harden SW, Johnson DN, Kimball AK, Sheng W, Smith JA, Scott KA, Frazier CJ, de Kloet AD, and Krause EG (2022). A Novel Organ-Specific Approach to Selectively Target Sensory Afferents Innervating the Aortic Arch. Front Physiol 13, 841078. 10.3389/fphys.2022.841078. [PubMed: 35399269]
19. Abraira VE, and Ginty DD (2013). The sensory neurons of touch. Neuron 79, 618–639. 10.1016/j.neuron.2013.07.051. [PubMed: 23972592]
20. Handler A, and Ginty DD (2021). The mechanosensory neurons of touch and their mechanisms of activation. Nat Rev Neurosci 22, 521–537. 10.1038/s41583-021-00489-x. [PubMed: 34312536]
21. Rutlin M, Ho CY, Abraira VE, Cassidy C, Bai L, Woodbury CJ, and Ginty DD (2015). The Cellular and Molecular Basis of Direction Selectivity of Adelta-LTMRs. Cell 160, 1027. 10.1016/j.cell.2015.02.013. [PubMed: 29698636]
22. Wende H, Lechner SG, Cheret C, Bourane S, Kolanczyk ME, Pattyn A, Reuter K, Munier FL, Carroll P, Lewin GR, and Birchmeier C (2012). The transcription factor c-Maf controls touch receptor development and function. Science 335, 1373–1376. 10.1126/science.1214314. [PubMed: 22345400]
23. Lou S, Duan B, Vong L, Lowell BB, and Ma Q (2013). Runx1 controls terminal morphology and mechanosensitivity of VGLUT3-expressing C-mechanoreceptors. J Neurosci 33, 870–882. 10.1523/JNEUROSCI.3942-12.2013. [PubMed: 23325226]
24. Chesler AT, Szczot M, Bharucha-Goebel D, Ceko M, Donkervoort S, Laubacher C, Hayes LH, Alter K, Zampieri C, Stanley C, et al. (2016). The Role of PIEZO2 in Human Mechanosensation. N Engl J Med 375, 1355–1364. 10.1056/NEJMoa1602812. [PubMed: 27653382]
25. Sharma N, Flaherty K, Lezgiyeva K, Wagner DE, Klein AM, and Ginty DD (2020). The emergence of transcriptional identity in somatosensory neurons. Nature 577, 392–398. 10.1038/s41586-019-1900-1. [PubMed: 31915380]
26. Molliver DC, Wright DE, Leitner ML, Parsadanian AS, Doster K, Wen D, Yan Q, and Snider WD (1997). IB4-binding DRG neurons switch from NGF to GDNF dependence in early postnatal life. Neuron 19, 849–861. 10.1016/s0896-6273(00)80966-6. [PubMed: 9354331]
27. Stucky CL, and Lewin GR (1999). Isolectin B(4)-positive and -negative nociceptors are functionally distinct. J Neurosci 19, 6497–6505. 10.1523/JNEUROSCI.19-15-06497.1999. [PubMed: 10414978]
28. Li L, and Ginty DD (2014). The structure and organization of lanceolate mechanosensory complexes at mouse hair follicles. Elife 3, e01901. 10.7554/eLife.01901. [PubMed: 24569481]
29. Lawson SN, Harper AA, Harper EI, Garson JA, and Anderton BH (1984). A monoclonal antibody against neurofilament protein specifically labels a subpopulation of rat sensory neurones. J Comp Neurol 228, 263–272. 10.1002/cne.902280211. [PubMed: 6434599]
30. Bai L, Lehnert BP, Liu J, Neubarth NL, Dickendesher TL, Nwe PH, Cassidy C, Woodbury CJ, and Ginty DD (2015). Genetic Identification of an Expansive Mechanoreceptor Sensitive to Skin Stroking. Cell 163, 1783–1795. 10.1016/j.cell.2015.11.060. [PubMed: 26687362]
31. Ghitani N, Barik A, Szczot M, Thompson JH, Li C, Le Pichon CE, Krashes MJ, and Chesler AT (2017). Specialized Mechanosensory Nociceptors Mediating Rapid Responses to Hair Pull. Neuron 95, 944–954 e944. 10.1016/j.neuron.2017.07.024. [PubMed: 28817806]
32. Li L, Rutlin M, Abraira VE, Cassidy C, Kus L, Gong S, Jankowski MP, Luo W, Heintz N, Koerber HR, et al. (2011). The functional organization of cutaneous low-threshold mechanosensory neurons. Cell 147, 1615–1627. 10.1016/j.cell.2011.11.027. [PubMed: 22196735]
33. Kalueff AV, Aldridge JW, LaPorte JL, Murphy DL, and Tuohimaa P (2007). Analyzing grooming microstructure in neurobehavioral experiments. Nat Protoc 2, 2538–2544. 10.1038/nprot.2007.367. [PubMed: 17947996]
34. Cavanaugh DJ, Chesler AT, Braz JM, Shah NM, Julius D, and Basbaum AI (2011). Restriction of transient receptor potential vanilloid-1 to the peptidergic subset of primary afferent neurons follows its developmental downregulation in nonpeptidergic neurons. J Neurosci 31, 10119–10127. 10.1523/JNEUROSCI.1299-11.2011. [PubMed: 21752988]
35. McCoy ES, Taylor-Blake B, and Zylka MJ (2012). CGRPalpha-expressing sensory neurons respond to stimuli that evoke sensations of pain and itch. PLoS One 7, e36355. 10.1371/journal.pone.0036355. [PubMed: 22563493]

36. Dubin AE, Murthy S, Lewis AH, Brosse L, Cahalan SM, Grandl J, Coste B, and Patapoutian A (2017). Endogenous Piezo1 Can Confound Mechanically Activated Channel Identification and Characterization. Neuron 94, 266–270 e263. 10.1016/j.neuron.2017.03.039. [PubMed: 28426961]
37. Kay AR, Alfonso A, Alford S, Cline HT, Holgado AM, Sakmann B, Snitsarev VA, Stricker TP, Takahashi M, and Wu LG (1999). Imaging synaptic activity in intact brain and slices with FM1–43 in C. elegans, lamprey, and rat. Neuron 24, 809–817. 10.1016/s0896-6273(00)81029-6. [PubMed: 10624945]
38. Bagriantsev SN, Gracheva EO, and Gallagher PG (2014). Piezo proteins: regulators of mechanosensation and other cellular processes. J Biol Chem 289, 31673–31681. 10.1074/jbc.R114.612697. [PubMed: 25305018]
39. Wu J, Lewis AH, and Grandl J (2017). Touch, Tension, and Transduction - The Function and Regulation of Piezo Ion Channels. Trends Biochem Sci 42, 57–71. 10.1016/j.tibs.2016.09.004. [PubMed: 27743844]
40. McMillin MJ, Beck AE, Chong JX, Shively KM, Buckingham KJ, Gildersleeve HI, Aracena MI, Aylsworth AS, Bitoun P, Carey JC, et al. (2014). Mutations in PIEZO2 cause Gordon syndrome, Marden-Walker syndrome, and distal arthrogryposis type 5. Am J Hum Genet 94, 734–744. 10.1016/j.ajhg.2014.03.015. [PubMed: 24726473]
41. Malecot CO, Bito V, and Argibay JA (1998). Ruthenium red as an effective blocker of calcium and sodium currents in guinea-pig isolated ventricular heart cells. Br J Pharmacol 124, 465–472. 10.1038/sj.bjp.0701854. [PubMed: 9647469]
42. Szallasi A, and Blumberg PM (1999). Vanilloid (Capsaicin) receptors and mechanisms. Pharmacol Rev 51, 159–212. [PubMed: 10353985]
43. Shin KC, Park HJ, Kim JG, Lee IH, Cho H, Park C, Sung TS, Koh SD, Park SW, and Bae YM (2019). The Piezo2 ion channel is mechanically activated by low-threshold positive pressure. Sci Rep-Uk 9. ARTN 6446 10.1038/s41598-019-42492-4.
44. Gale JE, Marcotti W, Kennedy HJ, Kros CJ, and Richardson GP (2001). FM1–43 dye behaves as a permeant blocker of the hair-cell mechanotransducer channel. J Neurosci 21, 7013–7025. 10.1523/JNEUROSCI.21-18-07013.2001. [PubMed: 11549711]
45. Truschel ST, Wang E, Ruiz WG, Leung SM, Rojas R, Lavelle J, Zeidel M, Stoffer D, and Apodaca G (2002). Stretch-regulated exocytosis/endocytosis in bladder umbrella cells. Mol Biol Cell 13, 830–846. 10.1091/mbc.01-09-0435. [PubMed: 11907265]
46. de Groat WC, Griffiths D, and Yoshimura N (2015). Neural control of the lower urinary tract. Compr Physiol 5, 327–396. 10.1002/cphy.c130056. [PubMed: 25589273]
47. Barry CM, Ji E, Sharma H, Yap P, Spencer NJ, Matusica D, and Haberberger RV (2018). Peptidergic nerve fibers in the urethra: Morphological and neurochemical characteristics in female mice of reproductive age. Neurourol Urodyn 37, 960–970. 10.1002/nau.23434. [PubMed: 29053899]
48. Bertrand MM, Korajkic N, Osborne PB, and Keast JR (2020). Functional segregation within the pelvic nerve of male rats: a meso- and microscopic analysis. J Anat 237, 757–773. 10.1111/joa.13221. [PubMed: 32598494]
49. Forrest SL, Osborne PB, and Keast JR (2014). Characterization of axons expressing the artemin receptor in the female rat urinary bladder: a comparison with other major neuronal populations. J Comp Neurol 522, 3900–3927. 10.1002/cne.23648. [PubMed: 25043933]
50. Giniatullin R (2020). Ion Channels of Nociception. Int J Mol Sci 21. 10.3390/ijms21103553.
51. Gaffield MA, Romberg CF, and Betz WJ (2011). Live imaging of bulk endocytosis in frog motor nerve terminals using FM dyes. J Neurophysiol 106, 599–607. 10.1152/jn.00123.2011. [PubMed: 21543750]
52. Li D, Herault K, Oheim M, and Ropert N (2009). FM dyes enter via a store-operated calcium channel and modify calcium signaling of cultured astrocytes. Proc Natl Acad Sci U S A 106, 21960–21965. 10.1073/pnas.0909109106. [PubMed: 20007370]
53. Hille B (1992). Ionic channels of excitable membranes, 2nd Edition (Sinauer Associates).
54. Romero LO, Massey AE, Mata-Daboin AD, Sierra-Valdez FJ, Chauhan SC, Cordero-Morales JF, and Vasquez V (2019). Dietary fatty acids fine-tune Piezo1 mechanical response. Nat Commun 10, 1200. 10.1038/s41467-019-09055-7. [PubMed: 30867417]

55. Marasco PD, Tsuruda PR, Bautista DM, Julius D, and Catania KC (2006). Neuroanatomical evidence for segregation of nerve fibers conveying light touch and pain sensation in Eimer's organ of the mole. Proc Natl Acad Sci U S A 103, 9339–9344. 10.1073/pnas.0603229103. [PubMed: 16751268]

56. Moroni M, Servin-Vences MR, Fleischer R, Sanchez-Carranza O, and Lewin GR (2018). Voltage gating of mechanosensitive PIEZO channels. Nat Commun 9, 1096. 10.1038/s41467-018-03502-7. [PubMed: 29545531]

57. Lukacs V, Mathur J, Mao R, Bayrak-Toydemir P, Procter M, Cahalan SM, Kim HJ, Bandell M, Longo N, Day RW, et al. (2015). Impaired PIEZO1 function in patients with a novel autosomal recessive congenital lymphatic dysplasia. Nat Commun 6, 8329. 10.1038/ncomms9329. [PubMed: 26387913]

58. Dhaka A, Uzzell V, Dubin AE, Mathur J, Petrus M, Bandell M, and Patapoutian A (2009). TRPV1 is activated by both acidic and basic pH. J Neurosci 29, 153–158. 10.1523/JNEUROSCI.4901-08.2009. [PubMed: 19129393]

59. Marshall KL, Clary RC, Baba Y, Orlowsky RL, Gerling GJ, and Lumpkin EA (2016). Touch Receptors Undergo Rapid Remodeling in Healthy Skin. Cell Rep 17, 1719–1727. 10.1016/j.celrep.2016.10.034. [PubMed: 27829143]

60. Chaplan SR, Bach FW, Pogrel JW, Chung JM, and Yaksh TL (1994). Quantitative assessment of tactile allodynia in the rat paw. J Neurosci Methods 53, 55–63. 10.1016/0165-0270(94)90144-9. [PubMed: 7990513]

Highlights

- FM 1–43 is a fluorescent dye that labels mouse sensory neurons *in vivo*
- Sensory neuron FM 1–43 labeling requires the activity of the mechanosensor PIEZO2
- FM 1–43 reveals a PIEZO2-dependent urethral neuron that is engaged during urination
- This dye is a useful tool for identifying when and where PIEZO2 is active *in vivo*

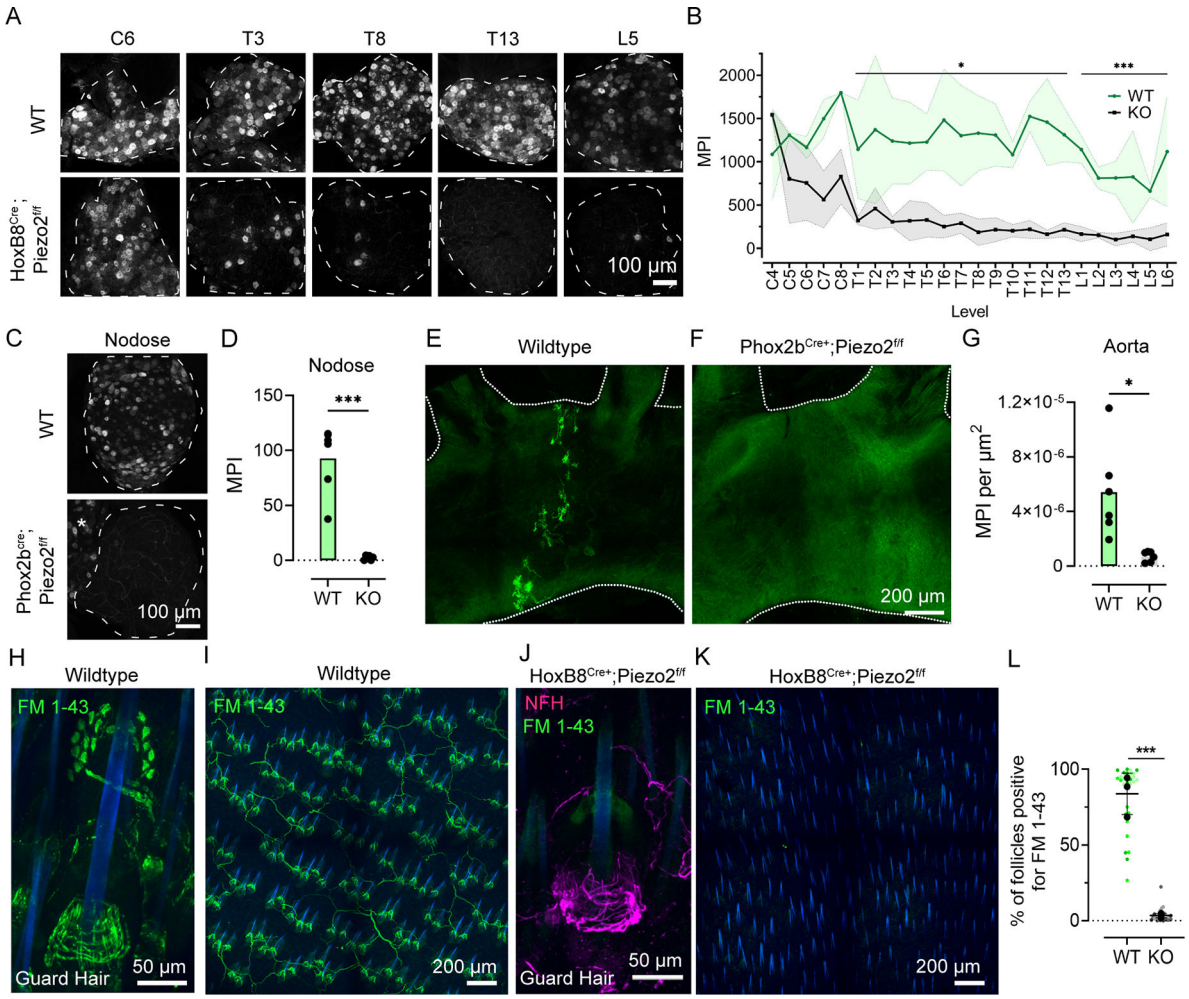

Figure 1: The majority of FM 1–43 sensory neuron uptake depends on *Piezo2* expression

(A) Representative z-stack images of whole-mount dorsal root ganglia DRG from wildtype (Top) or *HoxB8^{Cre+};Piezo2$^{f/f}$* (Bottom) mice that were injected i.p. with FM 1–43 24 h prior. The DRG level written on the top applies to both images underneath it. Scale bar applies to all images. Tissue area outlined with dashed line.

(B) Mean pixel intensity (mean pixel intensity, abbreviated as MPI) of FM 1–43 labeling in DRGs at different vertebral level from wildtype (N=3, 2 female and 1 male) and *HoxB8^{Cre+};Piezo2$^{f/f}$* KO animals(N=4, 2 male, 2 female). Center line is mean, with shaded areas representing SD. A mean pixel intensity value was calculated per animal, per region, and mean thoracic (p=0.02, *) and mean lumbar (p=0.0021, **) values were significantly lower in KO compared to WT (N=3–4 per group). Means were analyzed by Welch's two-tailed t test.

(C) Representative z-stacks of whole-mount nodose ganglion from wildtype (Top) and *Phox2b^{Cre+};Piezo2$^{f/f}$* mice injected i.p. with FM 1–43 24 h prior. Asterisk marks the jugular ganglion, which is fused to the nodose in mice. Nodose area outlined with dashed line. Scale bar applies to both images.

(D) MPI of FM 1–43 labeling in left and right nodose ganglia from wildtype (N= 3, 1 male and 2 female) and *Phox2b^{Cre+};Piezo2$^{f/f}$* (N=3, 2 male and 1 female) animals. Individual

dots represent values from each ganglion, two values per mouse. Means from each condition were analyzed by a Welch's two-tailed t-test, p=0.0008 (***).

(E) Representative 24 h FM 1–43 labeling of whole-mount aorta baroreceptor endings in wildtype and (F) *Phox2b*$^{Cre+}$;*Piezo2*$^{f/f}$ KO mouse. Scale bar: 200 μm.

(G) MPI of FM 1–43 of the aortic arch between the left subclavian and left common carotid artery from wildtype (N= 3, 1 male and 2 female) and *Phox2b*$^{Cre+}$;*Piezo2*$^{f/f}$ (N=3, 2 male and 1 female) animals. Individual dots represent area normalized values from each field of view, two values (front and back) per mouse. Means from all animals in each condition were analyzed using a Welch's two-tailed t-test, p=0.0198 (*).

(H) Representative z-stack image of 24 h FM 1–43 labeling of cutaneous neurons around a guard hair in whole-mount skin from wildtype mouse. Hair shaft autofluorescence is shown in blue. Some Merkel cells (top of the hair shaft), longitudinal lanceolate, and circumferential endings (base of the hair shaft) are visibly labeled.

(I) Representative z-stack image of 24 h FM 1–43 labeling (green) of cutaneous neurons in whole-mount skin from wildtype animals. Hair shaft autofluorescence is shown in blue.

(J) Representative z-stack 24 h FM 1–43 labeling of whole-mount skin from *HoxB8*$^{Cre+}$;*Piezo2*$^{f/f}$ KO mouse immunostained for NFH (magenta).

(K) Representative z-stack image of 24 h FM 1–43 labeling (green) of cutaneous neurons in whole-mount skin from *HoxB8*$^{Cre+}$;*Piezo2*$^{f/f}$ KO animal.

(L) Quantification of the percent of follicles labeled with FM 1–43 from wildtype (N= 3, 3 female) and from (N= 3, 2 female and 1 male) *HoxB8*$^{Cre+}$;*Piezo2*$^{f/f}$ KO animals. Individual colored dots represent a single field of view, while black dots represent means from each animal. Means from all animals in each condition plotted ± S.D. and were analyzed using a Welch's two-tailed t-test, p=0.0005 (***).

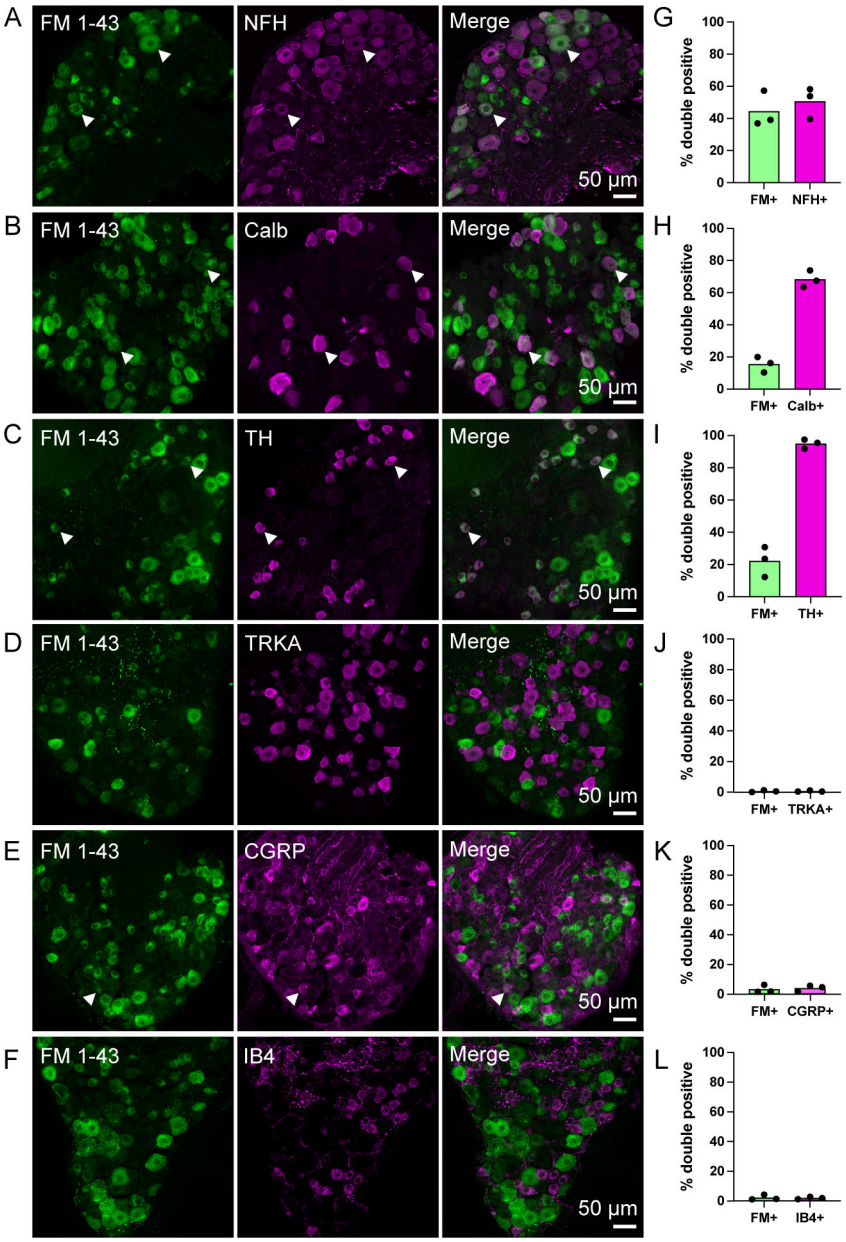

Figure 2: Characterization of DRG cell types that take up FM 1–43

(A-F) Representative z-stack images of immunostained DRG sections from wild-type mice injected i.p. with FM 1–43 48h prior. Arrowheads indicate examples of double positive cells where present. Scale bar applies to all images on the same row.

(G-L) Quantification of the percent of double positive cells from within the FM 1–43 positive population or double positive cells within the cell marker population in DRG sections from wildtype animals. N=3 mice, individual means from each shown as a single dot. Bars represent mean value from all three animals.

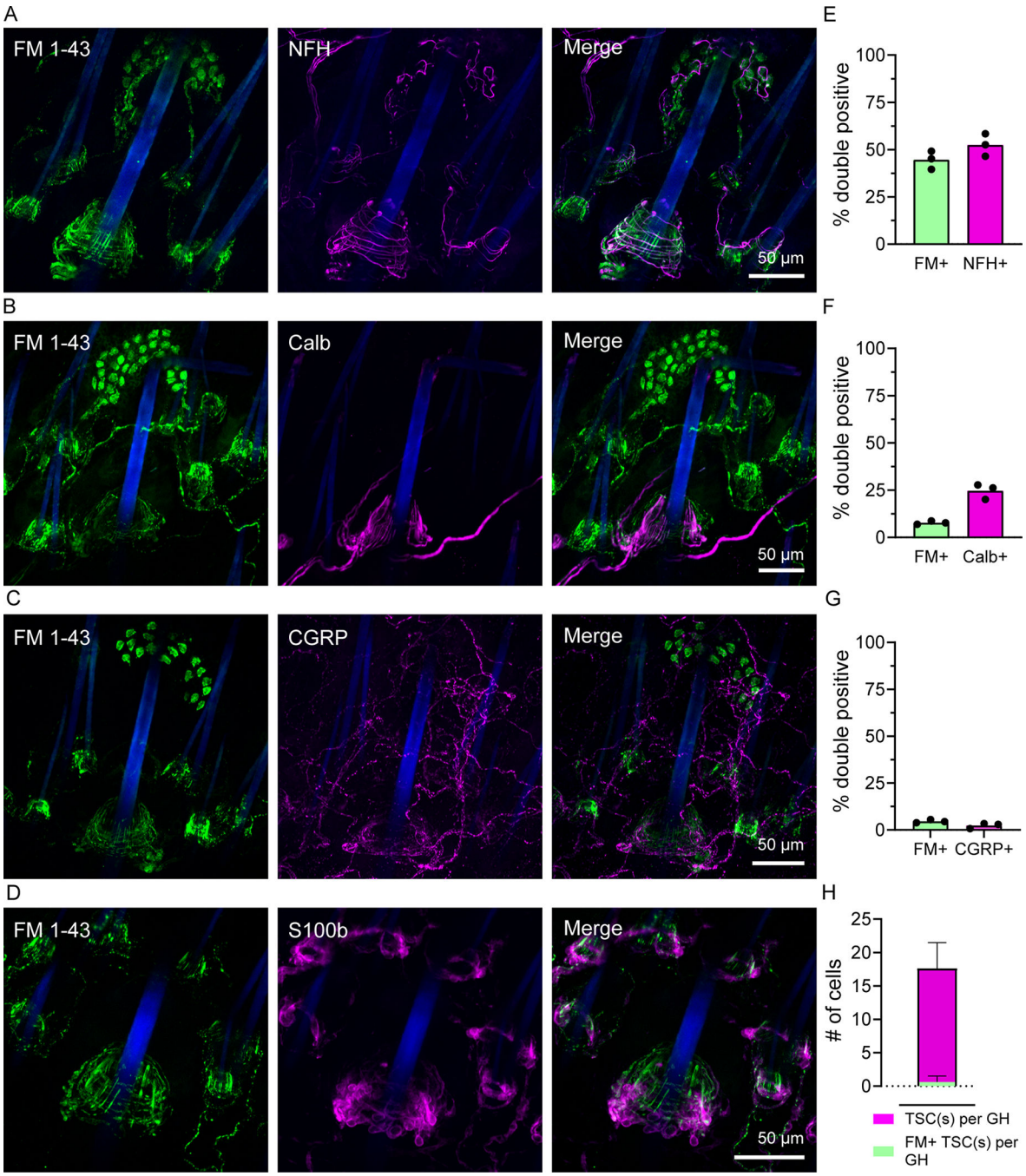

Figure 3: FM 1–43 uptake in cutaneous end organ structures

(A-D) Representative z-stack images of immunostained guard hairs in whole-mount skin from wild-type mice injected i.p. with FM 1–43 24h prior. FM 1–43 signal shown on left (green), immunostained marker shown in middle (magenta), and merged image shown on the right. Scale bar applies to all images on the same row.

(E-G) Quantification of the percent of double positive signal from within FM 1–43 (left bar) or marker positive (right bar) signal. N=3 female mice, 5–8 fields of view analyzed per

animal. Individual means from each animal shown as a single dot, Bars represent mean value from all three animals.

(H) Quantification of the Schwann cell colocalization with FM 1–43 signal near guard hairs. Magenta bar indicates the average count of TSCs per guard hair, green indicates the average number of TSCs colocalized with FM. N=3 female mice, 5–6 guard hairs analyzed per mouse plotted ± S.D.

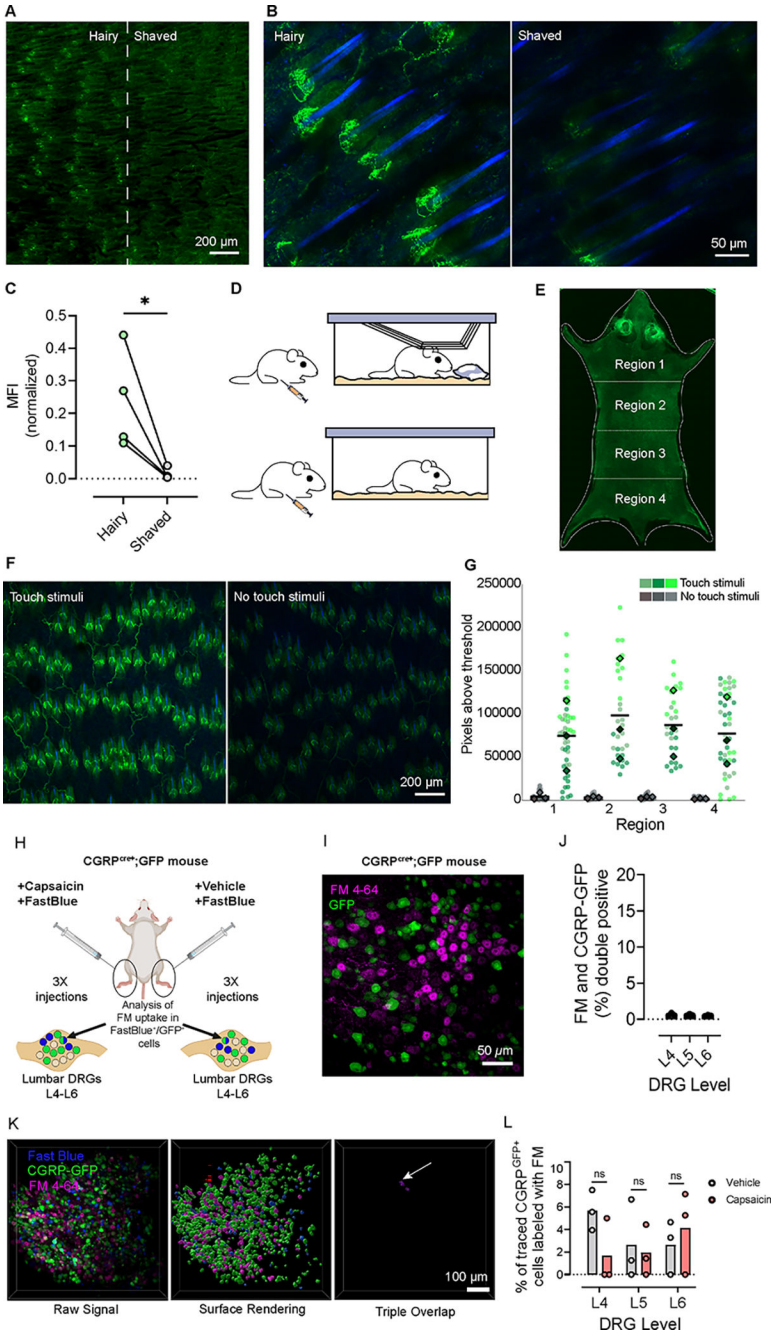

Figure 4: FM dyes label cutaneous end organ structures in an activity-dependent manner and do not label TRPV1 expressing neurons after capsaicin stimulus

(A) Low magnification z-stack image of FM 1–43 labeling of skin after dehairing, 16 h post i.p. FM 1–43 injection. The border of normal hairy (left) and depilated (right) hindlimb skin indicated by the dotted line.

(B) Higher magnification representative image of ‘Hairy’ (left) and ‘Shaved’ (right) hindlimb skin. Scale bar applies to both images.

(C) Quantification of the mean FM 1–43 fluorescence signal normalized to hair follicle count. Individual points represent mean values from 5 fields of view imaged from each condition, per mouse (N = 4 mice), analyzed using a paired *t*-test (p = 0.0487).
(D) Schematic diagram of mouse cage with 'Touch Stimuli' (top, wire cage bar and nestlet) and one with 'No touch stimuli' (bottom, no wire cage bar or nestlet).
(E) Widefield stitched image of whole dorsal back skin from a mouse at 25x. Dashed lines indicate regional distinctions used for analysis. Bright regions at the head are the autofluorescent ears: face and ear skin were not imaged at higher magnification for analysis.
(F) Representative z-stack images of dorsal skin with 'Touch Stimuli' (left) and with 'No touch stimuli' (right). Scale bar applies to both images.
(G) Quantification of the sum of pixels above a set threshold in each region. Colored dots represent each field of view analyzed and the corresponding colored diamond represents the mean from each animal. Means were analyzed using two-way ANOVA with Sidák's multiple comparisons test, and by this test treatment conditions were significantly different p=0.0340. Due to insufficient N to determine normality (N=3), we also ran the Mann-Whitney U test non-parametruc analysis which returned p = 0.1 However, the data shows a clear trend, which we speculate would be significant with higher N.
(H) Schematic diagram of attempt to achieve FM labeling of TRPV1 expressing neurons. $CGRP^{cre+}$;GFP mice were injected with FM 4–64, followed by 2 h waiting period. FastBlue and capsaicin/vehicle was co-injected subcutaneously intraplantar, near the proximal tibia, and lower biceps femoris. After 72 h, DRGs (L4-L6) were collected, fixed, and wholemount imaged.
(I) Representative z-stack of a lumbar DRG from a $CGRP^{cre+}$;GFP mouse, i.p. injected with FM 4–64 24 h prior. GFP (green) and FM 4–64 (magenta) channels are displayed as a single merged image.
(J) Quantification of overlap between FM 4–64 and GFP from $CGRP^{cre+}$;GFP mouse 72 h post i.p. FM 4–64 injection. Dots represent means from each vertebral level. N=3 DRGs analyzed per level.
(K) 3D representation of raw signal from an L6 DRG (top left) from a 'Vehicle' injected animal. Surface rendering of each channel (top right) and triple overlap (bottom) are shown using Imaris surface-surface colocalization tool. Arrow points to a confirmed instance of triple overlap. Scale bar applies to all images.
(L) Quantification of FM 4–64 labeling in DRGs expressed as a percent of $CGRP^{GFP}$/FastBlue-positive cells. N=3 animals (1 female and 2 male). Means from each DRG level (L4, L5, L6) are plotted and analyzed using a paired two-tailed t-test (p=0.184, 0.841, 0.613 respectively).

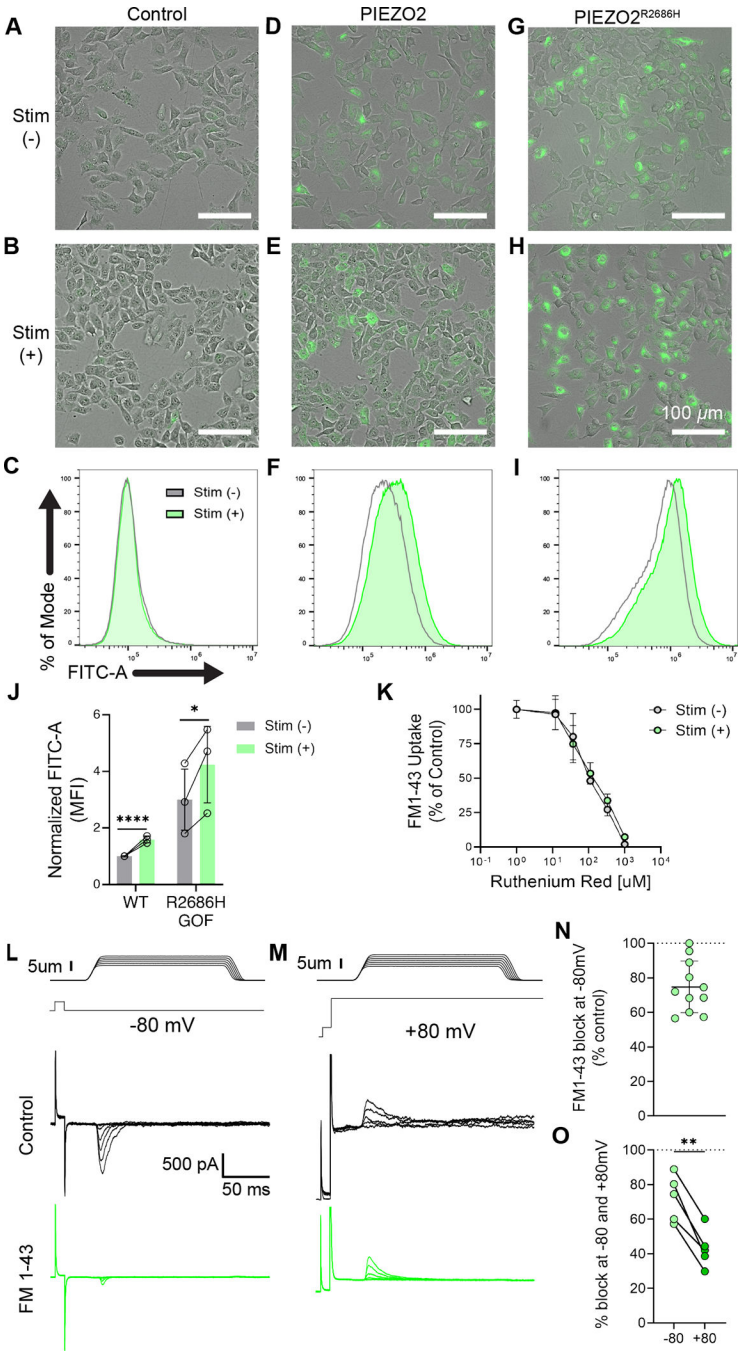

Figure 5: In cell culture, FM 1–43 labeling increases with human PIEZO2 channel activity

(A) Representative images from HEK P1KO cells that were transfected with control plasmid, exposed to FM 1–43, and had no stimulus. Scale applies to all images.

(B) HEK P1KO cells transfected with control plasmid and exposed to orbital shaking.

(C) Representative flow cytometry plots from HEK P1KO cells transfected with control plasmid. X-axis is FITC-A (log scale) and represents FM 1–43 loading; Y-axis is % cell count.

(D-E) Images from HEK P1KO cells transfected with *PIEZO2* with no stimulus(D) or (E) exposed to orbital shaking.
(F) Flow cytometry histograms of *PIEZO2* transfected HEK P1KO cells with (green) and without (gray) exposure to shaking, axes as in (C)
(G-H) Representative images and flow cytometry plots from HEK cells transfected with $PIEZO2^{R2868H}$, a gain-of-function allele, with no stimulus (G) and (H) exposed to orbital shaking.
(I) Representative flow cytometry histograms from HEK cells transfected with $PIEZO2^{R2868H}$ with (green) and without (gray) exposure to orbital shaking, axes as in (C)
(J) Flow cytometry quantification of each transfection condition with and without orbital shaking, normalized to control transfected cells. Averages are plotted from 3 biological replicates ± S.D. Analyzed using unpaired two-tailed *t*-test, PIEZO2 WT $p < 0.00001$ (****) and $PIEZO2^{R2686H}$ $p = 0.0475$ (*). Connecting lines indicate biological replicates run on same day.
(K) FM 1–43 uptake, shown as a percent of maximum, is suppressed in a concentration-dependent manner during exposure to ruthenium red (x-axis).
(L-M) Stimulus-dependent mechanically activated (poke) whole cell currents were acquired in 1 μm increments under control conditions (top, black traces) and in the presence of 10 μM FM 1–43 (bottom, green traces). Currents were recorded at either a holding potential of −80 mV (L) or +80 mV (M). Poker displacements are shown (up to 4 μm above threshold). Currents are leak subtracted relative to levels prior to the mechanical stimulus.
(N) Inhibition of hPIEZO2 mediated MA currents is plotted as a percent of control for n= 10 cells.
(O) When inhibition was possible to determine at +80 mV for an individual cell (n=5), the data from an individual cell is connected. Analyzed by two-tailed paired t-test, p=0.0015 (**).

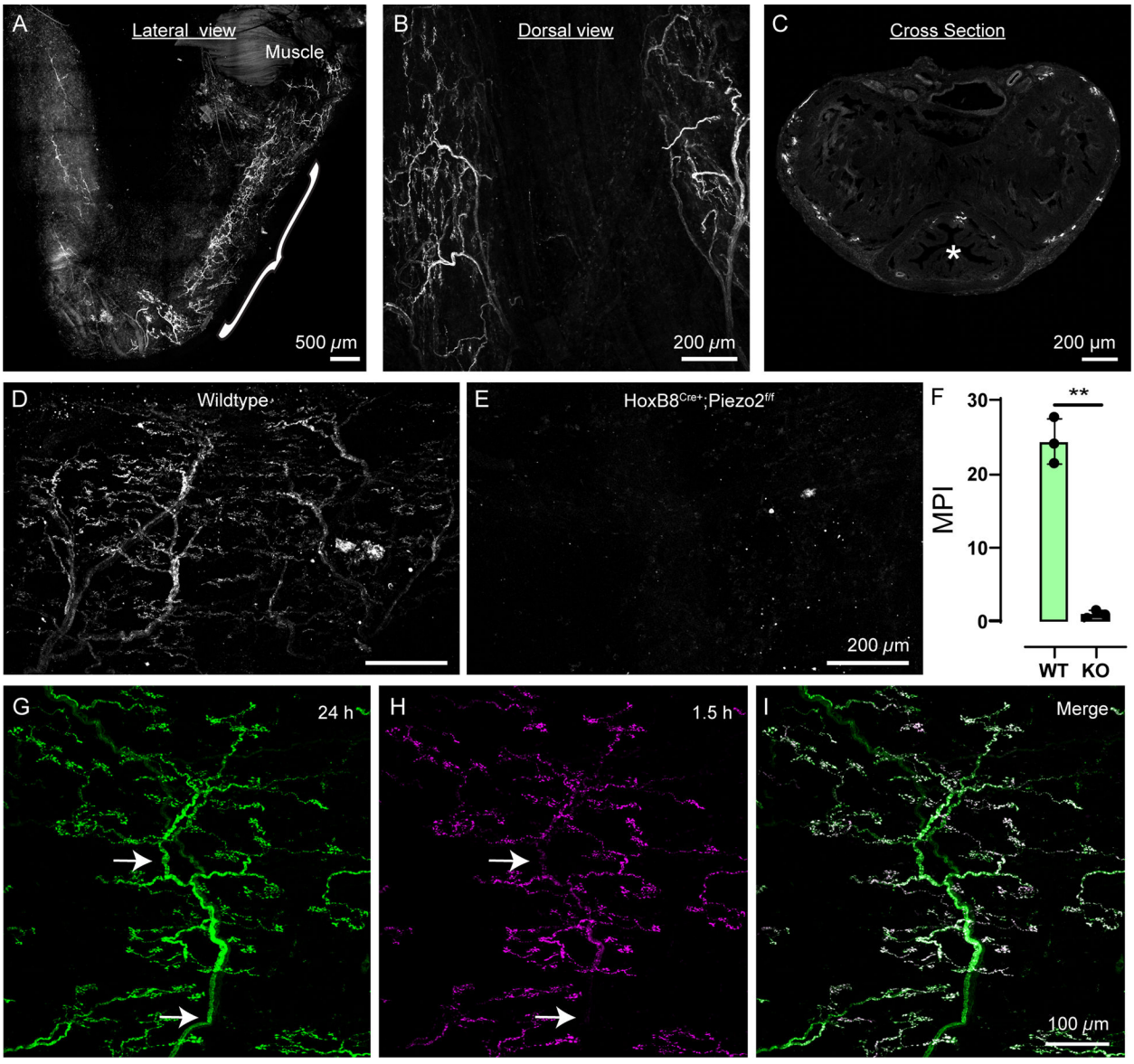

Figure 6: FM 1–43 reveals novel lateralized sensory endings in the pelvic urethra of male mice

(A) Lateral view of the male pelvic urethra labeled by FM 1–43 injection 24 h before tissue harvest. Bracket indicates pelvic urethra and area of urethral neuron labeling. Note free nerve endings in the most distal penile urethra.

(B) Dorsal view of the pelvic urethra.

(C) Cross-sectional view of the pelvic urethra shaft showing labeling around the edges. Urethral opening is marked by an asterisk.

(D) 24 h FM 1–43 labeling of neurons in a wildtype pelvic urethra.

(E) 24 h after FM 1–43 injection in a *HoxB8^{Cre+};Piezo2$^{f/f}$* KO mouse, the pelvic urethra shows no neuronal labeling.

(F) Mean pixel intensity of FM 1–43 labeling in pelvic urethra from wildtype (N= 3) and *HoxB8^{Cre+};Piezo2$^{f/f}$* KO (N=3) animals. Dots represent individual animals, data shown as

mean ± SD Means from all animals in each condition were analyzed using a Welch's two-tailed t-test, p=0.0049 (**).

(G) 24 h labeling of a urethral neuron ending shows nerve trunks (arrows).

(H) 1.5 h labeling of the same neuron ending in F with FM 4–64 only shows labeling on the "leaves" of the tree.

(I) Merged image from channels in G,H. White represents overlap.

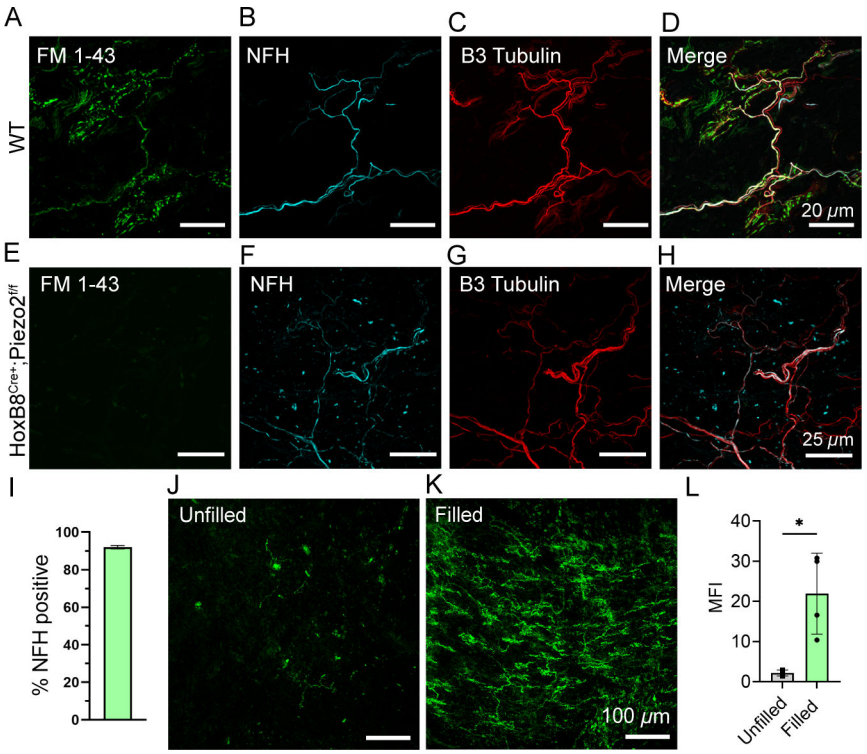

Figure 7: Characterization of tree-like urethral neuron endings, which are engaged during urination

(A-D) High magnification z-stack image of FM 1–43 labeling and immunostaining of a urethral ending in a wildtype animal, 24 h after injection.

(E-H) High magnification z-stack image of FM 1–43 labeling and immunostaining of a urethral ending in a *HoxB8*$^{Cre+}$*;Piezo2*$^{f/f}$ KO animal, 24 h after injection.

(I) Quantification of NFH-positive innervation of urethral neuron endings expressed as a percent. N=3 mice analyzed, 5–6 fields of view per animal. Data shown as mean ± SD.

(J) FM 1–43 labeling in the pelvic urethra when the bladder remains unfilled.

(K) FM 1–43 labeling of neuron endings in the pelvic urethra after 1 h of continuous bladder filling and recurring micturition cycles.

(L) Quantification of FM 1–43 labeling brightness (MPI) of endings in pelvic urethra in ‘Filled’ versus ‘Unfilled’ animals. Dots represent individual animals, data shown as mean ± SD. N=4 mice per condition were analyzed per condition using an unpaired t-test, $p < 0.024$ (*).

Key resources table

REAGENT or RESOURCE	SOURCE	IDENTIFIER
Antibodies		
Anti-neurofilament heavy	Abcam	RRID:AB_304560; Cat.# ab4680
anti-Calbindin D-28k	Swant	RRID:AB_100003; Cat.# CB-38a
anti-CGRP	Abcam	RRID:AB_114157; Cat.# ab47027
anti-S100b	Abcam	RRID:AB_882426; Cat.# ab52642
anti-beta III tubulin	Abcam	RRID:AB_444319; Cat.# AB_18207
anti-TH	Abcam	RRID:AB_152453; Cat.# ab76442
anti-TRKA	Biotechne R&D System	RRID:AB_228304; Cat.#AF1056-SP
anti-CGRP	Abcam	RRID:AB_165841; Cat.# ab81887
AlexaFluor 647	Invitrogen	RRID:AB_253586; Cat.# A21449
AlexaFluor 594	Invitrogen	RRID:AB_141637; Cat.# A21207
Isolectin GS-IB4 from *Griffonia simplicifolia*, Alexa Fluor™ 647 Conjugate	Thermo Fisher	RRID:SCR_014365; Cat.# I32450
Lycopersicon Esculentum (Tomato) Lectin, DyLight 649 Invitrogen	Invitrogen	Cat.# L32472
Chemicals, peptides, and recombinant proteins		
FM 1–43	Invitrogen	Cat.# T3163
FM 1–43FX	Invitrogen	Cat.# F35355
FM 4–64FX	Invitrogen	Cat.# F34653
Capsaicin	Sigma	Cat.# M2028
FastBlue tracer	Polysciences	Cat.# 17740–1
Ruthenium Red	Sigma	Cat.# R2751
ADVASEP-7	Biotium	Cat.# 70029
O.C.T.	Fisher Healthcare	Cat.# 23-730-571
Tissue Tek O.C.T.	Sakura	Cat.# 4583
Gold anti-fade mounting medium	Thermo Fisher	Cat.# S36939
Fluoromount G mounting medium with DAPI	Thermo Fisher	Cat.# 00-4959-52
Superfrost Plus microscope slides	Fisher	Cat.# 12-550-15
Lipofectamine 2000	Thermo Fisher	Cat.# 11668019
PEI MAX	Polysciences	Cat.# 24765
Dmem, high glucose, pyruvate	Thermo Fisher	Cat.# 11995073
Penicillin-Streptomycin (10,000 U/mL)	Thermo Fisher	Cat.# 15140122
Matrigel	Corning	Cat.# 354234

REAGENT or RESOURCE	SOURCE	IDENTIFIER
MEM (Minimum Essential Medium)	Thermo Fisher	Cat.# 11095080
Gibco Normal Goat Serum	Thermo Fisher	Cat.# PCN5000
Donkey Serum	Sigma	Cat.# D9663
Experimental models: Cell lines		
Neuro2A-P1ko	Gary Lewin[56]	N/A
Piezo1 knock-out HEK293T (HEK P1KO)	ATCC	Cat.# CRL-3519
Experimental models: Organisms/strains		
C57BL/6J	Jackson Laboratories	RRID:IMSR_JAX:000664
CGRP^{cre+};GFP	Mark J. Zylka[35]	N/A
HoxB8^{Cre+};Piezo2$^{f/f}$	Previously reported in [4]	N/A
Phox2b^{Cre}; Piezo2$^{f/f}$	Previously reported in [6]	N/A
Recombinant DNA		
hPIEZO2- codon-optimized-T2A-BFP-WPRE *("PIEZO2")*	This paper, Table S1	N/A
hPIEZO2-codon-optimized_mCherry-WPRE	This paper, Table S2	N/A
hPIEZO2_R2686H-codon-optimized-T2A-BFP-WPRE (*"PIEZO2^{R2686H}*)	This paper, Table S3	N/A
hPiezo1-pIRES2-EGFP	Previously reported in [57]	N/A
hPiezo1-pIRES2-tdTomato	This paper, Table S4	N/A
Rat TRPV1	Previously reported in [58]	N/A
Software and algorithms		
FIJI (ImageJ)	Schindelin et. al. (2012) doi: 10.1038/nmeth.2019	RRID:SCR_002285
Imaris (version 9.9.1)	Oxford Instruments	RRID:SCR_007370
Prism (GraphPad 9.2.0)	GraphPad Software	RRID:SCR_002798
Microsoft Excel	Microsoft	RRID:SCR_016137
FlowJo 10.7.2	BD	RRID:SCR_008520
Igor Pro 8.02	Wavemetrics	RRID:SCR_000325
pClamp software (version 10.7)	Molecular Devices	RRID:SCR_011323
Patchmaster	HEKA Elektronik	RRID:SCR_000034
Other		
EPC10 amplifier	HEKA Elektronik	N/A
HSPC-1	ALA Scientific Instruments	N/A
MultiClamp700A amplifier	Molecular Devices	N/A
DigiData1550	Molecular Devices	N/A